Formation of aluminosilicate-bearing quartz veins in the Simano nappe (Central Alps) : structural, thermobarometric and oxygen isotope constraints

Autor(en): **Allaz, Julien / Maeder, Xavier / Vannay, Jean-Claude**

Objekttyp: **Article**

Zeitschrift: **Schweizerische mineralogische und petrographische Mitteilungen = Bulletin suisse de minéralogie et pétrographie**

Band (Jahr): **85 (2005)**

Heft 2-3: **Central Alps**

PDF erstellt am: **27.04.2024**

Persistenter Link: https://doi.org/10.5169/seals-1660

Schweizerische Mineralogische und Petrographische Mitteilungen 85, 191–214, 2005

Formation of aluminosilicate-bearing quartz veins in the Simano nappe (Central Alps): structural, thermobarometric and oxygen isotope constraints

Julien Allaz[*,1], *Xavier Maeder*[*,2], *Jean-Claude Vannay*[*] and *Albrecht Steck*[*]

Abstract

We combined structural analysis, thermobarometry and oxygen isotope geochemistry to constrain the evolution of kyanite and/or andalusite-bearing quartz veins from the amphibolite facies metapelites of the Simano nappe, in the Central Alps of Switzerland. The Simano nappe records a complex polyphase tectonic evolution associated with nappe stacking during Tertiary Alpine collision (D1). The second regional deformation phase (D2) is responsible for the main penetrative schistosity and mineral lineation, and formed during top-to-the-north thrusting. During the next stage of deformation (D3) the aluminosilicate-bearing veins formed by crystallization in tension gashes, in tectonic shadows of boudins, as well as along shear bands associated with top-to-the-north shearing. D2 and D3 are coeval with the Early Miocene metamorphic peak, characterised by kyanite + staurolite + garnet + biotite assemblages in metapelites. The peak pressure (P) and temperature (T) conditions recorded are constrained by multiple-equilibrium thermobarometry at 630 ± 20 °C and 8.5 ± 1 kbar (~27 km depth), which is in agreement with oxygen isotope thermometry indicating isotopic equilibration of quartz-kyanite pairs at 670 ± 50 °C. Quartz-kyanite pairs from the aluminosilicate-bearing quartz veins yield equilibration temperatures of 645 ± 20 °C, confirming that the veins formed under conditions near metamorphic peak. Quartz and kyanite from veins and the surrounding metapelites have comparable isotopic compositions. Local intergranular diffusion in the border of the veins controls the mass-transfer and the growth of the product assemblage, inducing local mobilization of SiO_2 and Al_2O_3. Andalusite is absent from the host rocks, but it is common in quartz veins, where it often pseudomorphs kyanite. For andalusite to be stable at T_{max}, the pressure in the veins must have been substantially lower than lithostatic. An alternative explanation consistent with structural observations would be inheritance by andalusite of the kyanite isotopic signature during polymorphic transformation after the metamorphic peak.

Keywords: Aluminosilicate veins, thermobarometry, oxygen isotope geothermometry, Simano nappe, Central Alps.

Introduction

Aluminosilicate-bearing quartz veins (AbQ veins) are observed in amphibolite facies rocks of several orogens, including the Alps, the Himalayas, the Hellenides, and the North-American Cordillera (Klein 1976; Sauniac and Touret, 1983; Kerrick, 1988; Kerrick, 1990; Cavosie et al., 2002; Putlitz et al., 2002). Such AbQ veins reflect mobilization of SiO_2 and Al_2O_3 by fluids at ductile deformation conditions and can provide indications about the metamorphic conditions, the fluid sources, and the mechanism of vein formation (Cesare, 1994; Widmer and Thompson, 2001; Sepahi et al., 2004). Several recent studies demonstrated that AbQ veins are suitable for oxygen-isotope thermometry, and that they generally record near-peak, high-temperature (T) conditions (Cavosie et al., 2002; Putlitz et al., 2002).

Pre-Mesozoic and Mesozoic metapelites in the Central Alps commonly contain AbQ veins (Fig. 1). The Central Alps, also known as Lepontine domain, consist of a complex nappe stack that was metamorphosed under amphibolite-facies conditions. The studied area recorded 625 °C and 6.5 kbar (Engi et al., 1995; Todd and Engi, 1997). The AbQ veins, sometimes referred to as "Knauern" (German), often contain centimetre-size idiomorphic kyanite and/or andalusite crystals, and some spectacular samples are on exhibition in mineralogical collections throughout Europe. Aluminosilicate-bearing veins are widespread, especially

* Institute of Mineralogy and Geochemistry, University of Lausanne, 1015 Lausanne, Switzerland. <jean-claude.vannay@unil.ch>, <albrecht.steck@unil.ch>
[1] Present address: Institute of Geological Sciences, University of Berne, Baltzerstrasse 1-3, 3012 Bern, Switzerland. <jallaz@geo.unibe.ch>
[2] Institute for Geosciences, Johannes Gutenberg University, 55099 Mainz, Germany. <maederx@uni-mainz.de>

0036-7699/05/0085/191

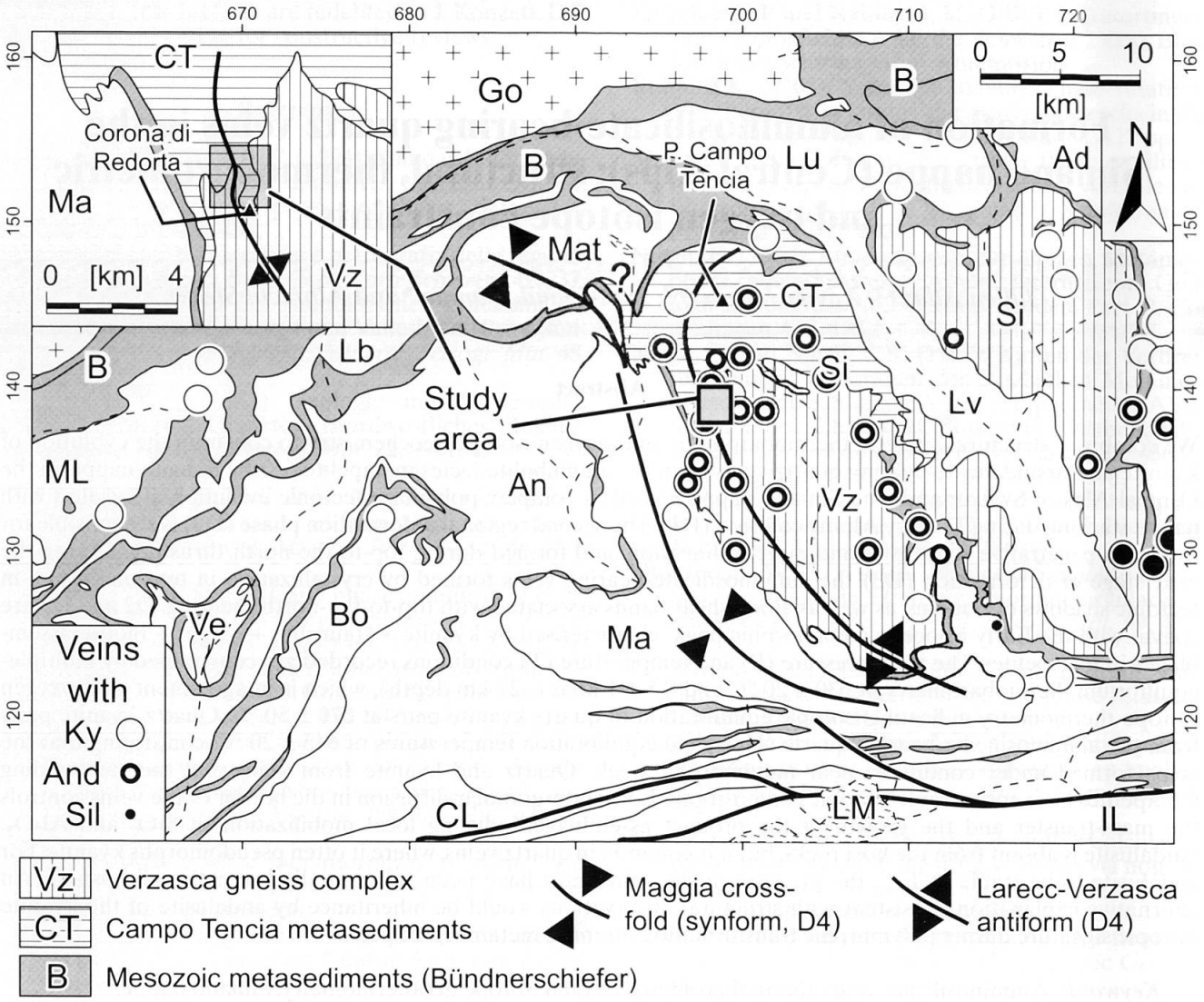

Fig. 1 Simplified structural map of the Central Alps showing the distribution of aluminosilicate-bearing veins. Numbers correspond to Swiss topographic coordinates. Lower Penninic units in white and above the Insubric / Canavese Line (IL / CL). Dashed lines are rivers and gray box in the middle indicates study area, enlarged in inset. Abbreviations: Ad — Adula, An — Antigorio, Bo — Bosco serie, CT — Campo Tencia, Go — Gotthard massif, LM — Lago Maggiore, Lu — Lucomagno, Lv — Leventina, Ma — Maggia, Mat — Matorello, ML — Monte Leone, Si — Simano, Ve — Verampio, Vz — Verzasca. Modified after Spicher (1972) and Keller et al. (1980). Aluminosilicates-vein locations from Klein (1976). Mineral abbreviations according to Kretz (1983).

in ductilely deformed paragneiss, as tension gashes or between segments of boudinaged layers (Preiswerk, 1918; Keller, 1968; Klein, 1976; Thompson, 1976; Codoni, 1981; Kerrick, 1988, 1990). The regional distribution of the type of aluminosilicate polymorph in the veins correlates with the peak metamorphic conditions in the surrounding rocks (Klein, 1976). In the kyanite zone of the Central Alps, both veins and surrounding gneisses contain kyanite, whereas kyanite + andalusite in the veins is found in the middle part of the Central Alps, and sillimanite is only observed in veins and country rocks of the more restricted sillimanite zone. The studied area is situated in the zone of the kyanite + andalusite veins described by Klein (1976) and Kerrick (1988) and in the SW of the region investigated by Keller (1968).

Kerrick (1990) presents a review of investigations on the AbQ veins in the Central Alps and elsewhere in regional metamorphic terranes. Almost all the described veins have been interpreted as a result of a process of infiltration metasomatism (cavity filling segregation), where the veins form by interaction and reaction between the host rock and a pervading fluid. Material of the host rock is dissolved, transported by advection to the fracture and repricipated due to fluid oversaturation. Keller (1968), Klein (1976) and Kerrick (1988) proposed such a model for the AbQ veins in the Central Alps, including the stud-

ied area. The biotite-rich border zone of the veins is interpreted to represent the residual part of the host rock, which has been depleted in silica, aluminium and alkaline elements by aqueous fluids to form the AbQ veins. Cesare (1994) proposed a process of syn-metamorphic veining for andalusite-biotite-quartz veins in pelitic hornfelses in the contact aureole of the Vedrette di Reis pluton. The veins are interpreted to form by hydrofracturing due to devolatilization reactions in the adjacent host pelite. Local intergranular diffusion controlled the mass-transfer, and the growth of the product assemblage of dehydratation is coeval in the vein and the host rock. Widmer and Thomson (2001) showed that the kyanite veins in the eclogite of the Zermatt-Saas zone are also locally derived, with a process of diffusive mass transfer of Al_2O_3 and SiO_2 through stagnant fluid.

A puzzling feature of AbQ in the Central Alps is that they often contain andalusite, whereas this aluminosilicate is lacking in the surrounding rocks. Kerrick (1990) proposed that andalusite formed in the AbQ veins in the Central Alps in response to a localised drop in P within the veins. Another interesting issue is the origin of the fluids responsible for the formation of the veins in amphibolite-facies conditions. Field observations and petrological evidence strongly suggest that the AbQ veins result from a localised Si and Al mobilization by metamorphic fluids (Keller, 1968). These hypotheses for the formation of aluminosilicate-bearing veins in the Central Alps are based essentially on detailed field investigations, and they remain largely untested by quantitative analytical results. As a consequence, the kinematic and metamorphic significance of AbQ veins within the framework of the evolution of the Campo Tencia unit in the Simano nappe is still poorly constrained, notably because of lacking data on their geochemical composition and the metamorphic conditions they record. The aim of this study is to quantitatively address the evolution of AbQ veins from a representative area of the Central Alps, selected for its abundance of kyanite and andalusite-bearing veins. For this purpose, we combined detailed geological mapping, structural analysis, petrographic study, multiple-equilibrium thermobarometry, and oxygen isotope geochemistry of the veins as well as the surrounding gneisses.

Geological setting

The deepest part of the Alpine nappe stack is exposed in a large-scale metamorphic dome in the Central Alps (Spicher, 1972; Trümpy, 1980; Escher et al., 1993; Steck et al., 2001). This so-called Lepontine dome is composed of several nappes cropping out between the Insubric Line to the south and the external crystalline Gotthard massif to the north (Fig. 1). The nappes in the Lepontine Alps are mainly composed of strongly deformed granitic gneisses derived from Caledonian or Hercynian basement rocks, interspersed with metasediments, probably derived from pre-Triassic sediments (Köppel et al., 1980). During the Alpine orogeny, these units have been metamorphosed under amphibolite-facies conditions, and the Lepontine metamorphic dome is characterised by a broadly concentric pattern of Barrovian staurolite to sillimanite isograds, cross-cutting the main tectonic contacts of the nappes (e.g. Wenk and Keller, 1969; Wenk, 1970; Spicher, 1972; Engi et al., 1995; Frey and Ferreiro-Mählmann, 1999). Despite its apparent simplicity, the metamorphic zoning in the Lepontine Alps is the consequence of a complex metamorphic history, characterised by U–Pb monazite ages at about 22 Ma in the region of interest (Köppel et al., 1980; Engi et al., 1995).

The investigated area is located in the Simano nappe (Keller, 1968; Keller et al., 1980). Geographically, this region is situated in the Maggia Valley (Ticino, Switzerland), on a high-altitude meadow called Alpe Larecc (commune of Prato-Sornico). Detailed geological mapping reveals that the area is composed of two distinct lithostratigraphic units (Fig. 2a). The upper unit is the Campo Tencia unit, dominated by amphibolite facies micaschists and paragneisses, which are interlayered at various scales. At the base of the Campo Tencia unit, metasediments discordantly overlie a layer of amphibolite a few tens of meters thick. In places, intercalations of micaschist and paragneiss occur within the amphibolite. This mafic layer could represent either a sill emplaced between the basement and the overlying sedimentary cover, or a lava flow. The basement, formed by the Verzasca complex, is composed of porphyroclastic granitic gneisses that are highly sheared near the contact with the overlying unit (border facies, Fig. 2a). The main structural features of the area are kilometre-scale N–S oriented late folds, such as the Larecc antiform (Fig. 2b). These folds are related to the Maggia cross-fold (Fig. 1), a major N–S oriented synform (Steck, 1998). The folds indicate an unusual E–W directed shortening, contrasting with most N–S Alpine structures, which formed during thrusting and folding related to S- to SE-directed subduction of the European plate under the Adriatic plate, and subsequent continental collision (Steck, 1998). The meaning of large-scale N–S oriented folds in the Central Alps is subject to debate. Grujic and Mancktelow

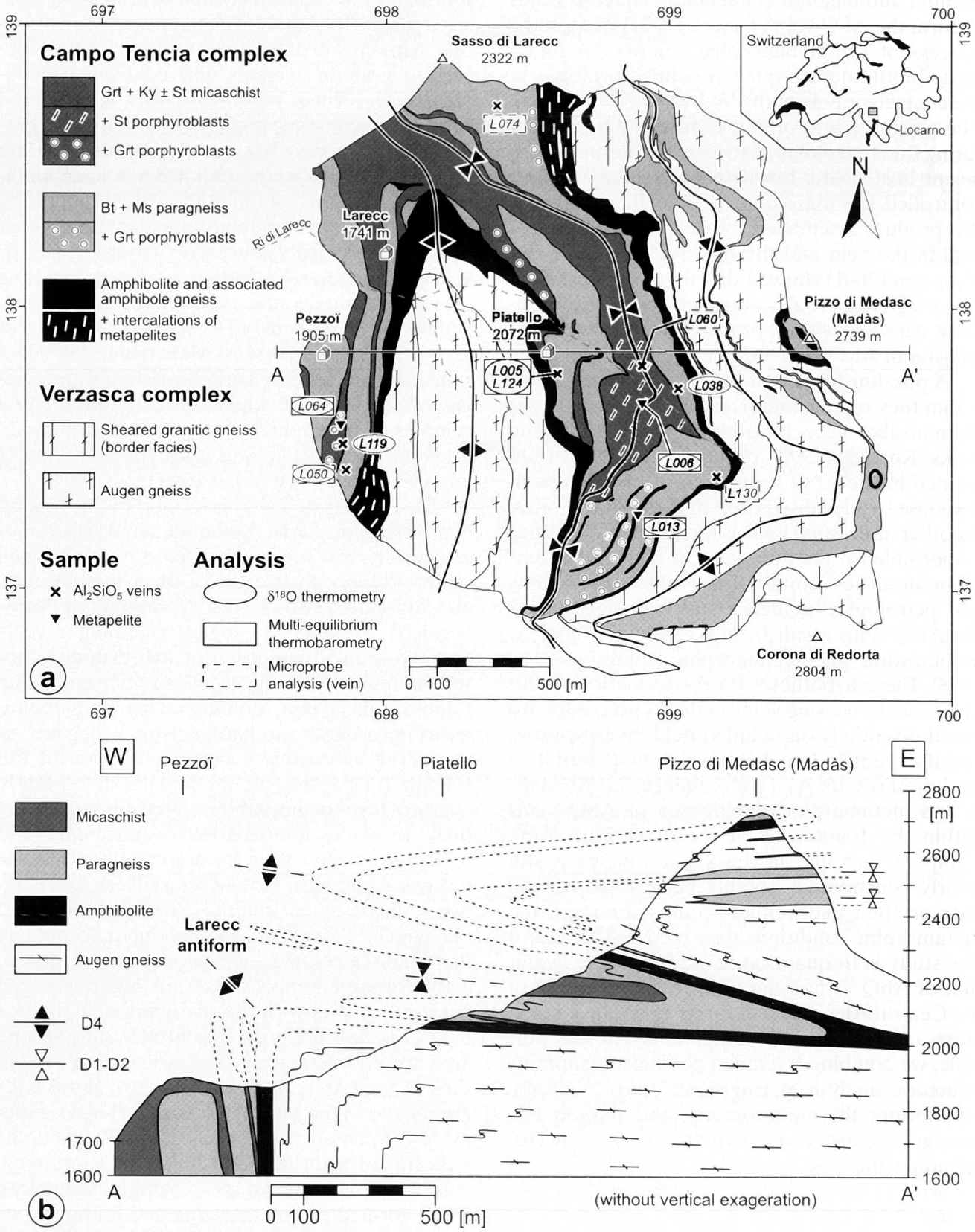

Fig. 2 (a) Geological map of Alpe Larecc (Val Maggia, Ticino, Switzerland). Numbers besides map are Swiss topographic coordinates. (b) Cross section A–A'. The large-scale structure of the studied area is dominated by the late N–S oriented Larecc antiform, related to large-scale cross folding in the Central Alps (Maggia Nappe; Steck, 1998). D1–D2 folds are revealed by repetitions of paragneiss layers in augen gneiss, like at the Pizzo di Medasc.

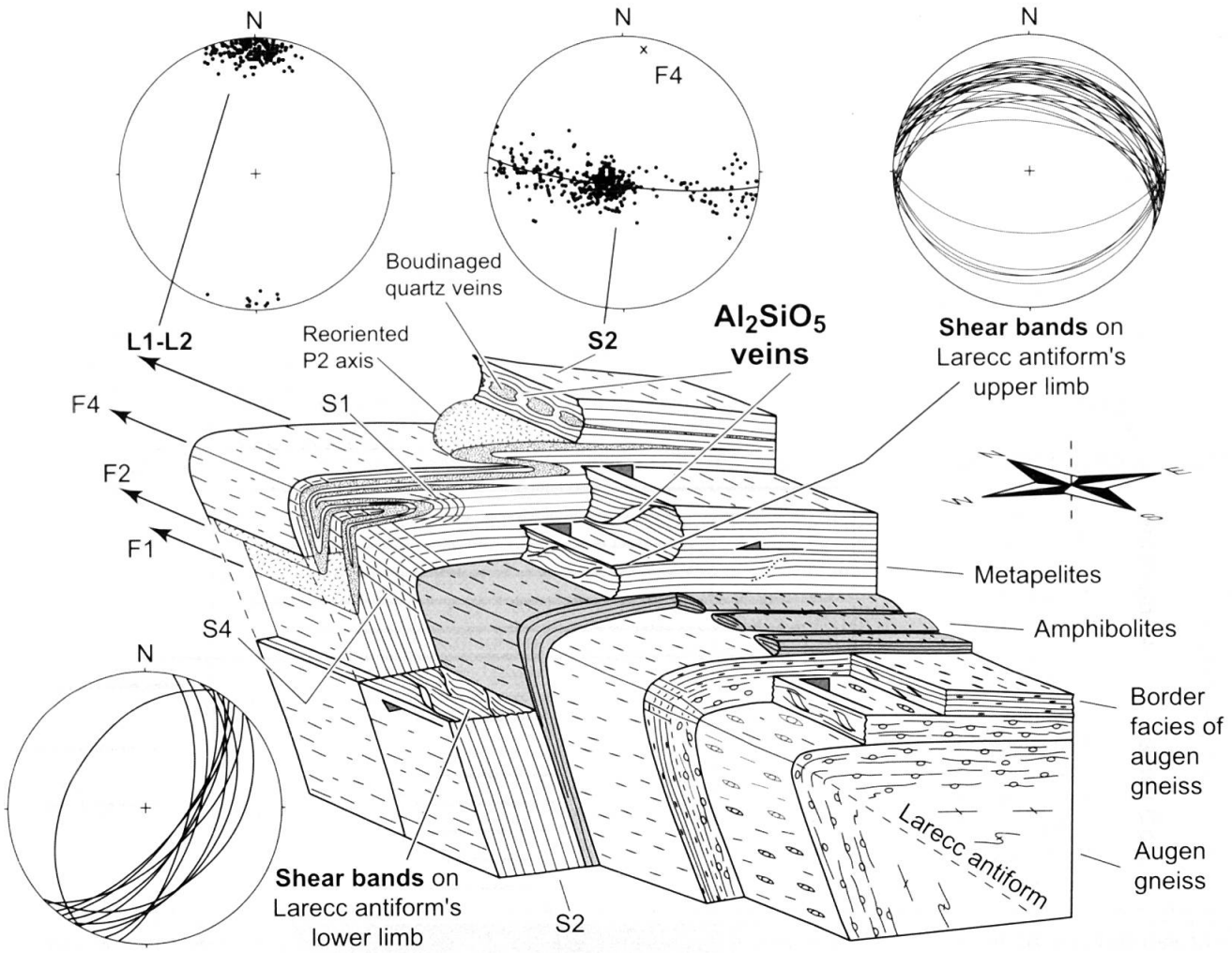

Fig. 3 Ductile structures in the Verzasca Complex and Campo Tencia unit at Alpe Larecc. The structural orientations are presented in equal-area stereograms (lower hemisphere). The diagram summarises the style and relative chronological relations of the various structures (not to scale). The aluminosilicate-bearing quartz veins occur mainly in metapelitic layers as tension gashes either along top-to-the-north shear bands, or between boudins in quartz veins. F — fold-axial plane, S — schistosity, L — lineation. See text for explanations.

(1996) and Maxelon (2004) interpret the Maggia unit as a steep zone separating the Antigorio nappe from the overlying Simano nappe. According to these authors, the Larecc antiform is a second order fold related to a larger antiform forming the Simano nappe. In contrast, Steck (1998) considers the Maggia unit a large-scale synform associated with a late phase of folding also responsible for creation of the Larecc antiform.

Structural evolution

The Central Alps show evidence of a complex polyphase structural evolution (specifically for the study area: Huber et al., 1980; Simpson, 1982; Merle and Le Gal, 1988; Grujic and Mancktelow, 1996; Steck, 1998). A detailed structural analysis has been performed in the study area to constrain the relative timing of deformation phases, and to correlate this evolution with the regional tectonic framework. These results allow us to place formation of the aluminosilicate-bearing veins within the kinematic evolution of the Campo Tencia unit in the Simano nappe.

The ductile structural evolution of Alpe Larecc is the result of five deformation phases (Table 1, Fig. 3). The first deformation phase (D1) is responsible for isoclinal folding associated with a penetrative schistosity marked by muscovite and biotite. Because D1 structures have been largely transposed during regionally dominant D2, they can only be distinguished in the hinge zones of D2 folds. The D1 structures most likely do not represent the earliest deformation, as an earlier schistosity is observed further north in the region (Nabholz and Voll, 1963; Steck, 1984; Délèze, 1999). However, in rocks of higher metamorphic grade, such as these in the study area, this earlier deformation is difficult to distinguish.

Table 1 Chronology of deformation and crystallization. F — fold, S — schistosity, L — lineation.

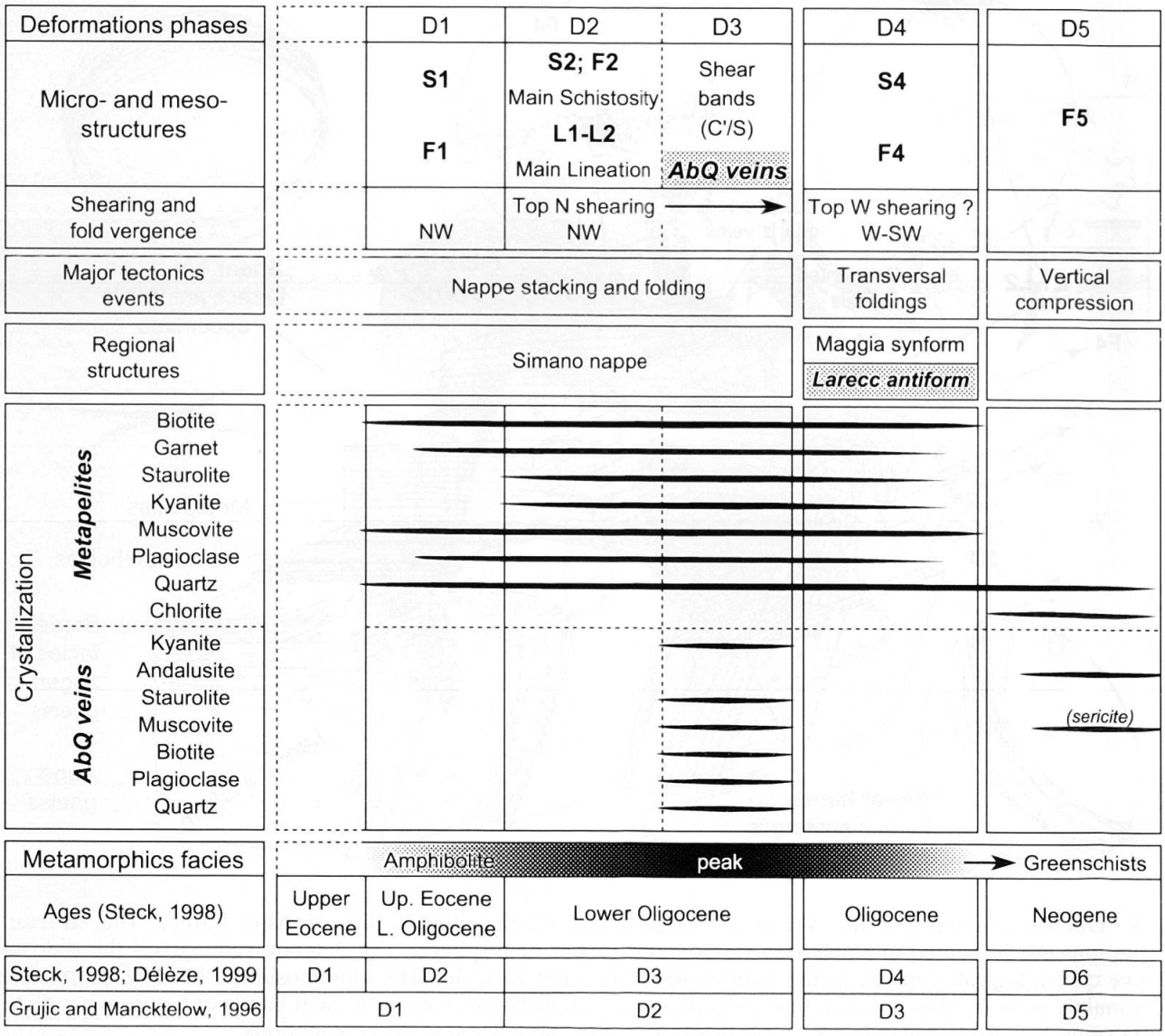

The second deformation phase (D2) is responsible for the main penetrative schistosity (S2) and mineral lineation (L2). D2 phase structures cannot always be distinguished from the strongly transposed D1 phase structures. S2 is also defined by muscovite and biotite whereas the L2 lineation is best recorded by kyanite in the metasediments, by hornblende in the amphibolites, and by stretched aggregates of K-feldspar and quartz in the granitic gneisses (Table 1). The L2 lineation shows a very consistent N–S orientation. Sigmoidal inclusion trails in syn–kinematic garnet and staurolite in the metasediments of the Campo Tencia unit, as well as K-feldspar delta and sigma clasts in the augengneiss of the Verzasca Complex, all indicate a top-to-the-north sense of shear. In some layers of the Campo Tencia unit, a post-kinematic growth of staurolite and kyanite is indicated by randomly oriented porphyroblasts, overgrowing the S2 schistosity. These observations indicate that high-T mineral growth near thermal peak outlasted the D2 phase of deformation. D2 is accompanied by intense folding producing isoclinal folds. Such folds are common at small scale (centimetre to meter), but they are also responsible for lithological repetitions at larger scale (Fig. 2b). The superposition of D2 on D1 folds resulted in a type 3 interference patterns (Ramsay, 1967). On the regional scale D2 folds verge towards the N to NW, and they are likely related to the N- to NW-directed emplacement of nappe structures in the Central Alps (e.g. Grujic and Mancktelow, 1996; Steck, 1998). At Alpe Larecc, the D2 fold axes are generally oriented N–S, parallel to a transposed stretching lineation L1–L2, although rare E–W fold-axial orientations are also observed. This suggests that the D2 folds have been largely reoriented during later deformation.

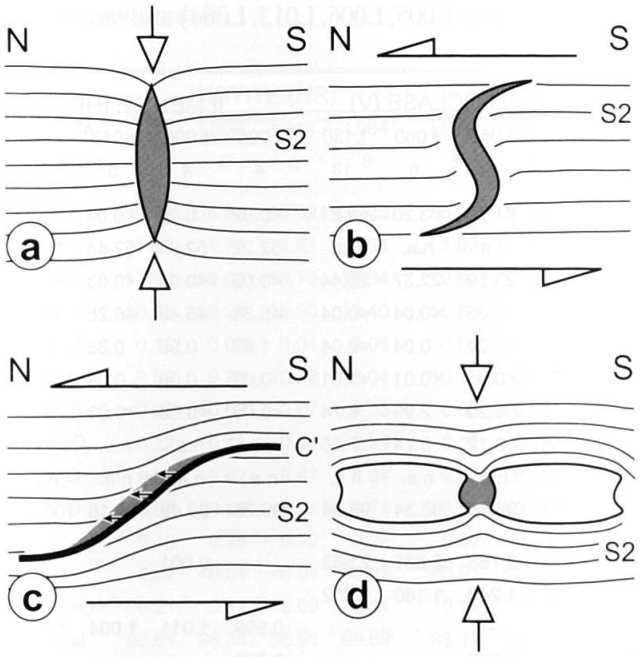

Fig. 4 Observed geometries of aluminosilicate-bearing veins (in grey). (a) Symmetric extensional fractures in rocks. (b) Sigmoidal tension gashes indicating top-to-the-north sense of shearing. (c) Extensional fractures along top-to-the-north C' shear bands. (d) Infilling in boudin necks of older quartz veins oriented parallel to the main S2 foliation. All veins show a N–S direction of opening.

The D3 phase is characterised by C'–S shear bands recording predominantly a top-to-the-north shearing. Less common top-to-the-south conjugate shear bands imply that D3 deformation involved a significant component of pure shear, combined with the dominant top-to-the-north simple shear. The AbQ veins always crosscut the penetrative S2 schistosity and they are frequently developed along top-to-the-north shear bands (Fig. 4), suggesting that they are coeval with the D3 deformation phase. Amphibolite facies conditions prevailed during D2–D3 indicated by the growth of kyanite both in the veins and the surrounding metasediments. D2 and D3 are related to burial and nappe emplacement in the Central Alps (Grujic and Mancktelow, 1996; Steck, 1998).

Late folds deforming both the main penetrative schistosity and the AbQ veins reflect D4 deformation. It forms the main large-scale structure of the study area, the Larecc antiform (Fig. 2b, 3). D4 fold axes are consistently N–S oriented and verge west. In the Campo Tencia metasediments, a penetrative S4 axial cleavage developed in the hinge zone of D4 folds, whereas only a coarser crenulation cleavage is observed in the more competent granitic gneiss of the Verzasca complex (Fig. 3). S4 foliation is marked by muscovite and biotite, together with staurolite and kyanite in micaschists, which indicates that D4 took place under amphibolite-facies conditions, in agreement with the conclusions of Wenk and Keller (1969) and Steck (1998) for the regional tectono-metamorphic evolution. The N–S fold axial orientation and W-directed vergence of the D4 folds contrast significantly with the dominant N- to NW-directed thrusting and folding in the Central Alps. Grujic and Mancktelow (1996) interpret D4 to be coeval with the creation of Simano fold-nappe. However, our analysis shows that D4 folds deform the D2 and D3 structures related to nappe stacking (Figs. 2b, 3), indicating that D4 deformation post-dates the main phase of nappe emplacement in the Central Alps.

We consequently interpret D4 deformation as recording a late phase of E–W directed shortening, following the N- to NW-directed phase of nappe stacking in the Central Alps. This interpretation implies that D4 "cross-folding" producing the Larecc antiform is coeval with formation of the N–S oriented Maggia synform (Steck, 1998).

Analytical conditions

Chemical compositions of minerals from four metapelites (L005, L006, L013, L064) have been obtained by *in situ* analysis on a Cameca SX-50 microprobe of the Institute of Mineralogy and Geochemistry of the University of Lausanne. Complementary analysis on vein minerals from four samples (L050, L060, L074 and L130) have been obtained on a JEOL JXA-8200 microprobe of the Institute of Geological Sciences of the University of Berne. In both cases, analytical conditions were 15kV and 20nA with a minimum beam size for garnet, staurolite, aluminosilicates and ilmenite. To minimise volatilization of alkalis, plagioclase and micas have been analysed using a lower current (10 nA) and a slightly defocused beam. Results from both instruments overlap within analytical error. All analyses are presented in Table 2 (mineral abbreviations after Kretz (1983)).

Host rock petrography

Micaschists, paragneiss and amphibolite of the Campo Tencia complex contain diagnostic amphibolite-facies assemblages, with estimated metamorphic equilibrium conditions at 625 °C and 6.5 kbar (Engi et al., 1995; Todd and Engi, 1997). Amphibolites marked in Figure 2 (more than 50% amphibole) are often associated with amphibolite-bearing gneiss alternating at millimetre- to decametre-scale. Moreover, intercalations of micaschist or paragneiss are also observed (Fig. 2a).

Table 2 Microprobe analyses of minerals in metapelite host rock (samples L005, L006, L013, L064) and vein (samples L074, L050, L060, L130).

	GARNET (HR)				PLAGIOCLASE (HR)				PLAGIOCLASE (V)				ILMENITE (HR)			
Sample	L005	L006	L013	L064	L005	L006	L013	L064	L074	L050	L060	L130	L005	L006	L013	L064
Nbr of pts	18	4	4	4	11	5	3	4	6	12	6	13	4	4	5	5
SiO_2	37.04	37.37	37.45	37.16	62.45	64.98	65.08	62.82	63.66	61.78	63.20	58.81	<0.02	0.05	<0.04	<0.04
TiO_2	0.02	0.05	0.05	0.03	n.a.	n.a.	n.a.	n.a.	n.a.	n.a.	n.a.	n.a.	52.22	52.94	52.44	53.12
Al_2O_3	20.58	20.51	20.65	20.53	22.53	21.53	21.76	23.18	23.22	23.59	22.37	25.44	<0.02	<0.03	<0.03	<0.03
FeO	35.27	37.18	37.23	35.66	<0.06	<0.06	0.06	0.08	<0.04	0.05	<0.04	<0.04	45.38	45.48	46.26	46.31
MnO	1.38	1.07	0.13	0.82	<0.05	n.a.	n.a.	n.a.	<0.04	<0.04	0.04	<0.04	1.62	0.95	0.38	0.85
MgO	3.18	3.66	3.65	3.30	<0.02	n.a.	n.a.	n.a.	<0.01	<0.01	<0.01	<0.01	0.03	0.06	0.08	<0.03
CaO	2.72	1.24	1.76	2.81	3.80	2.59	2.75	4.66	4.09	4.20	2.99	6.74	<0.05	<0.03	<0.03	<0.03
Na_2O	n.a.	n.a.	n.a.	n.a.	9.50	10.28	10.11	9.08	9.06	9.12	9.74	7.65	n.a.	n.a.	n.a.	n.a.
K_2O	n.a.	n.a.	n.a.	n.a.	0.12	0.11	0.10	0.11	0.10	n.a.	n.a.	n.a.	n.a.	n.a.	n.a.	n.a.
Total	100.19	101.08	100.92	100.31	98.40	99.49	99.86	99.93	100.13	98.74	98.34	98.64	99.25	99.48	99.16	100.28
Si	2.975	2.979	2.985	2.980	2.797	2.870	2.868	2.782	2.814	2.763	2.831	2.653	-	0.001	-	-
Al	1.947	1.927	1.939	1.938	1.189	1.121	1.130	1.209	1.210	1.243	1.180	1.352	-	-	-	-
Ti	0.001	0.003	0.003	0.002	-	-	-	-	-	-	-	-	0.999	1.011	1.004	1.006
Fe^{3+}	0.102	0.110	0.086	0.101	-	-	0.002	0.003	-	0.002	-	-	0.003	-	-	-
Fe^{2+}	2.266	2.368	2.394	2.288	-	-	-	-	-	-	-	-	0.962	0.966	0.985	0.976
Mn	0.094	0.072	0.009	0.056	-	-	-	-	-	-	0.001	-	0.035	0.020	0.008	0.018
Mg	0.381	0.435	0.434	0.394	-	-	-	-	-	-	-	-	0.001	0.002	0.003	-
Ca	0.234	0.106	0.150	0.241	0.182	0.123	0.130	0.221	0.194	0.201	0.143	0.326	-	-	-	-
Na	-	-	-	-	0.825	0.880	0.864	0.779	0.776	0.791	0.845	0.669	-	-	-	-
K	-	-	-	-	0.007	0.006	0.006	0.006	0.006	-	-	-	-	-	-	-
Sum	8.000	8.000	8.000	8.000	5.000	5.000	5.000	5.000	5.000	5.000	5.000	5.000	2.000	2.000	2.000	2.000
Fe*	0.861	0.851	0.851	0.858												
Ca/Ca+Na					0.181	0.123	0.131	0.221	0.200	0.203	0.145	0.328				

	STAUROLITE (HR)				STAUROLITE (V)		
Sample	L005	L006	L013	L064	L074	L050	L060
Nbr of pts	5	4	7	3	4	9	16
SiO_2	27.24	27.02	26.95	27.65	28.11	27.04	27.61
TiO_2	0.60	0.69	0.48	0.81	0.52	0.63	0.55
Al_2O_3	53.65	54.10	53.16	53.24	55.17	54.65	54.33
FeO	12.44	13.26	14.16	13.19	10.39	12.31	12.52
MnO	0.26	0.13	0.06	0.07	0.23	0.15	0.22
MgO	1.38	1.38	1.73	1.75	1.27	1.43	1.39
CaO	<0.04	<0.04	<0.04	0.04	<0.01	<0.01	<0.01
Na_2O	<0.05	<0.05	<0.05	<0.05	0.12	0.04	<0.01
ZnO	n.a.	0.19	0.12	0.39	1.94	0.62	0.14
H_2O	2.07	2.09	2.09	2.10	2.12	2.10	2.10
Total	97.66(*)	98.86	98.77	99.26	99.87	98.97	98.86
Si	7.887	7.742	7.735	7.898	7.960	7.780	7.897
Al	18.309	18.270	17.982	17.923	18.411	18.236	18.316
Ti	0.131	0.149	0.104	0.174	0.110	0.133	0.119
Fe^{3+}	-	-	0.331	-	-	0.029	0.025
Fe^{2+}	3.013	3.178	3.068	3.151	2.460	3.042	2.970
Mn	0.064	0.032	0.015	0.017	0.054	0.041	0.053
Mg	0.596	0.589	0.740	0.745	0.535	0.659	0.591
Zn	n.a.	0.040	0.025	0.082	0.406	0.074	0.029
Ca	-	-	-	0.010	-	-	-
Na	-	-	-	-	0.064	0.006	-
Sum	30.000	30.000	30.000	30.000	30.000	30.000	30.000
Fe*	0.835	0.844	0.821	0.809	0.821	0.823	0.835

For Ilm, St, Ky, And, Ms and Bt, a representative average of several points is given. For the zoned Pl and Grt, only an average of rim composition is given (for typical Grt and Pl zoning, see Figs. 7 and 8). Minerals are normalized as follows:

- Grt: 12 O and 8 cat.
- Ilm: 3 O and 2 cat.
- Pl: 8 O and 5 cat.
- Ky, And: 5 O and 3 cat.
- St: 46 O and 30 cat. (+ 4 OH-group)
- Ms, Bt: 11 O and 7 or 8 cat. (+ 2 OH-group)

Abbreviations:
HR – Host Rock;
V – Vein;
n.a. – not analysed;
Fe* – $Fe^{tot}/(Fe^{tot}+Mg)$;
(*) Zn not analysed.

Table 2 (continued)

	BIOTITE (HR)				BIOTITE (V)				MUSCOVITE (HR)				MUSCOVITE (V)			
Sample	L005	L006	L013	L064	L074	L050	L060	L130	L005	L006	L013	L064	L074	L050	L060	L130
Nbr of pts	5	4	5	8	3	4	14	7	5	5	5	5	12	5	15	10
SiO_2	35.62	35.57	35.92	36.20	35.96	35.94	35.36	36.20	46.37	46.68	46.90	46.57	46.22	45.07	45.89	45.88
TiO_2	1.87	1.74	1.81	2.04	1.99	1.80	1.39	1.86	0.56	0.51	0.55	0.60	0.19	0.20	0.44	0.45
Al_2O_3	17.93	19.03	18.70	18.84	19.65	20.04	20.53	20.05	34.51	35.87	35.01	35.42	37.27	37.25	37.47	36.97
FeO	20.05	19.26	19.00	19.40	16.80	19.08	19.00	18.42	1.01	0.85	1.15	1.02	0.72	1.22	0.73	0.84
MnO	0.12	0.07	0.04	0.05	0.08	0.04	0.10	0.12	<0.04	<0.04	<0.04	<0.04	0.07	<0.04	<0.04	<0.04
MgO	9.63	9.72	10.32	10.04	10.10	9.11	9.24	9.60	0.86	0.66	0.94	0.75	0.52	0.39	0.43	0.49
CaO	<0.03	<0.03	0.07	<0.03	0.02	<0.01	0.01	<0.01	<0.03	<0.04	<0.04	<0.05	<0.01	0.02	<0.01	<0.01
Na_2O	0.22	0.48	0.31	0.39	0.11	0.35	0.17	0.22	1.35	1.95	1.93	1.49	1.42	1.53	1.86	1.22
K_2O	9.30	8.62	8.87	8.84	9.57	9.09	9.31	9.45	9.47	8.63	8.64	9.37	9.55	9.45	8.83	9.98
H_2O	3.58	3.69	3.74	3.74	3.59	3.71	3.71	3.67	4.46	4.53	4.52	4.52	4.57	4.53	4.56	4.55
F	0.48	0.28	0.22	0.26	0.52	0.31	0.25	0.41	<0.20	<0.20	<0.20	<0.20	<0.20	<0.20	<0.20	<0.20
Cl	0.02	<0.01	<0.01	<0.01	<0.01	<0.01	0.05	0.05	<0.01	<0.01	<0.01	<0.01	<0.01	<0.01	<0.01	<0.01
F,Cl=O	0.21	0.12	0.09	0.11	0.22	0.13	0.12	0.18	-	-	-	-	-	-	-	-
Total	98.61	98.34	98.91	99.69	98.17	99.34	99.00	99.87	98.59	99.68	99.64	99.74	100.53	99.66	100.21	100.38
Si	2.802	2.793	2.800	2.806	2.814	2.798	2.757	2.798	3.116	3.088	3.105	3.088	3.033	2.982	3.015	3.021
Ti	0.111	0.103	0.106	0.119	0.117	0.105	0.081	0.108	0.028	0.025	0.027	0.030	0.009	0.010	0.022	0.022
Al	1.663	1.762	1.718	1.721	1.813	1.839	1.888	1.826	2.734	2.797	2.733	2.768	2.883	2.906	2.903	2.869
Fe^{3+}	-	-	-	-	-	-	-	-	-	-	-	-	0.011	0.068	0.002	0.038
Fe^{2+}	1.319	1.264	1.239	1.257	1.099	1.242	1.240	1.190	0.057	0.047	0.064	0.057	0.029	-	0.039	0.008
Mn	0.008	0.005	0.003	0.003	0.005	0.003	0.007	0.008	-	-	-	-	0.004	-	-	-
Mg	1.129	1.137	1.199	1.160	1.178	1.057	1.075	1.106	0.082	0.065	0.093	0.074	0.051	0.038	0.042	0.048
Ca	-	-	0.006	-	0.002	-	0.001	-	-	-	-	-	-	0.001	-	-
Na	0.034	0.073	0.047	0.059	0.017	0.053	0.025	0.033	0.175	0.250	0.248	0.191	0.180	0.197	0.237	0.156
K	0.933	0.863	0.882	0.874	0.955	0.903	0.926	0.931	0.808	0.728	0.730	0.792	0.800	0.798	0.740	0.838
H	1.879	1.930	1.945	1.935	1.871	1.925	1.931	1.893	2.000	2.000	2.000	2.000	2.000	2.000	2.000	2.000
F	0.119	0.070	0.055	0.065	0.129	0.075	0.063	0.101	-	-	-	-	-	-	-	-
Cl	0.003	-	-	-	-	-	0.006	0.006	-	-	-	-	-	-	-	-
Sum	8.000	8.000	8.000	8.000	8.000	8.000	8.000	8.000	7.000	7.000	7.000	7.000	7.000	7.000	7.000	7.000
Fe*	0.539	0.526	0.508	0.520	0.482	0.540	0.536	0.518	0.410	0.420	0.408	0.435	0.440	0.641	0.494	0.489
K/K+Na									0.822	0.744	0.746	0.806	0.816	0.802	0.757	0.843

	KYANITE (HR)			KYANITE (V)				ANDALUSITE (V)							
Sample	L006	L013	L064	L074	L050	L060	L130	L074		L050		L060		L130	
Nbr of pts	4	9	4	8	8	10	20	8	2	5	5	10	7	2	2
Zone								Rim	Core	Rim	Core	Rim	Core	Rim	Core
SiO_2	36.34	36.14	36.53	37.50	36.23	36.64	36.74	37.06	37.20	35.59	36.18	36.20	36.21	36.44	36.34
TiO_2	0.01	0.01	<0.01	0.03	0.02	0.01	0.03	0.02	0.06	0.03	0.06	0.02	0.04	0.02	0.05
Al_2O_3	62.98	62.69	63.02	62.42	63.55	63.26	63.07	62.06	61.36	63.42	62.58	63.25	62.78	62.90	62.19
Fe_2O_3	0.19	0.14	0.15	0.12	0.19	0.15	0.18	0.21	1.05	0.28	0.91	0.23	0.51	0.19	0.81
MnO	<0.04	<0.04	0.07	<0.04	0.06	<0.04	<0.04	<0.04	0.04	<0.04	0.04	0.04	<0.04	<0.04	0.05
MgO	<0.01	<0.01	<0.01	0.02	<0.01	<0.01	<0.01	0.04	0.38	0.04	0.31	0.04	0.12	0.04	0.24
Total	99.52	98.98	99.77	100.09	100.05	100.06	100.02	99.39	100.09	99.36	100.08	99.78	99.67	99.59	99.68
Si	0.984	0.984	0.987	1.012	0.976	0.987	0.991	1.006	1.006	0.965	0.976	0.978	0.980	0.987	0.985
Al	2.012	2.013	2.008	1.984	2.019	2.010	2.004	1.987	1.957	2.026	1.991	2.014	2.004	2.007	1.987
Ti	<0.001	<0.001	-	<0.001	<0.001	<0.001	0.001	<0.001	0.001	0.001	0.001	<0.001	0.001	<0.001	0.001
Fe^{3+}	0.004	0.003	0.003	-	0.004	0.003	0.004	0.002	0.021	0.006	0.019	0.005	0.010	0.004	0.016
Fe^{2+}	-	-	-	0.003	-	-	-	0.003	-	-	-	-	-	-	-
Mn	-	-	0.002	-	0.001	-	-	-	0.001	-	0.001	0.001	-	-	0.001
Mg	-	-	-	<0.001	-	-	-	0.002	0.015	0.002	0.012	0.002	0.005	0.002	0.010
Sum	3.000	3.000	3.000	3.000	3.000	3.000	3.000	3.000	3.000	3.000	3.000	3.000	3.000	3.000	3.000

The mineralogy of amphibole-bearing rocks is generally dominated by tschermakitic to pargasitic hornblende, associated with plagioclase (oligoclase to andesine), quartz, garnet, ± biotite and accessory ilmenite, rutile and titanite. Muscovite may additionally be present in the more gneissic layers. Amphibole and garnet form millimetre-sized idiomorphic grains, whereas poikiloblastic plagioclase is elongated parallel to the main (S2) schistosity. The augen gneiss found in the eastern part of the study area (Fig. 2) mainly consists of quartz, plagioclase (albite to oligoclase), K-feldspars, biotite, muscovite and relics of garnet in feldspars causing a pale rose colour of this mineral at the outcrop. Ilmenite, rutile, apatite and zircon are found as accessory phases.

Micaschist and paragneiss consist of quartz, plagioclase, muscovite, biotite, garnet, kyanite and staurolite, with ilmenite, rutile, tourmaline, apatite, zircon and monazite as accessories. Mica and aluminosilicates are less abundant in the paragneiss. The modal composition of micaschist is: 30–60 vol% muscovite, 10–45% quartz, 10–20% biotite, 3–15% plagioclase, 1–3% garnet, 1–2% staurolite and 1–2% kyanite. In the paragneiss the quartz is more abundant (60–95%). Muscovite and biotite contents vary from 2 to 20% and 5 to 25%. Garnet is relatively rare (1–2%) and kyanite and staurolite generally do not exceed 1%. Some micaschist and paragneiss layers contain garnet porphyroblasts, 5 to 10 mm across (Fig 2a). Such lithologies have not only a higher garnet content (5–10%), but also contain more kyanite (2–3%) and staurolite (5–7%). Centimetre-sized staurolite porphyroblast occur locally in micaschist layers (Fig. 2a). Such staurolite-rich layers have a high muscovite content which gives a typical silver rock patina.

Biotite, muscovite, kyanite and staurolite mark the main S2 schistosity. However, staurolite usually is randomly oriented, indicating post-D2 crystallization, which is particularly common in the micaschist with cm-sized porphyroblast of staurolite. Helicitic inclusion trails in garnet and in some staurolite show a syn-tectonic growth during D1–D3 associated with a top to the north

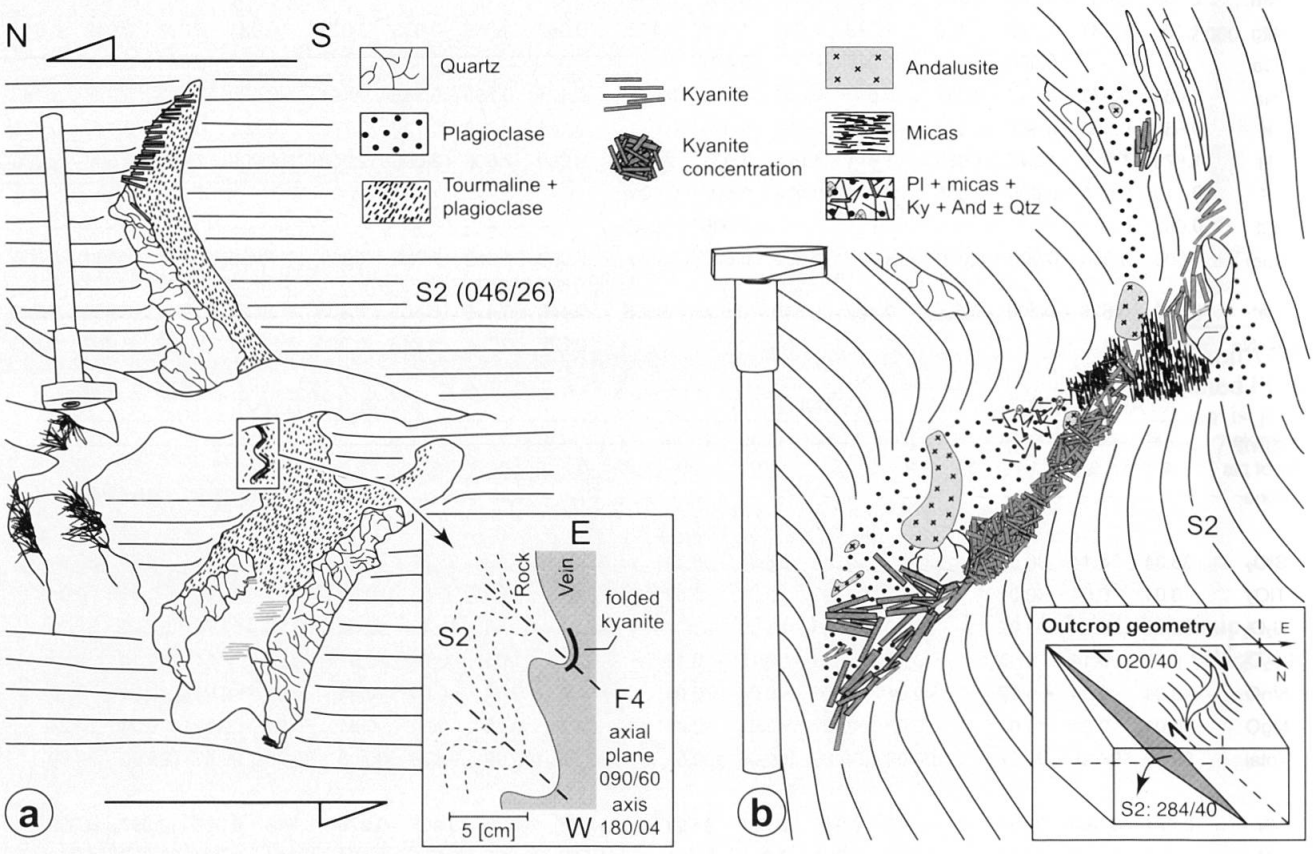

Fig. 5 Two examples of sigmoidal veins (D3 phase, Fig. 2b) with a top-to-the-north sense of shear, showing relations between D2, D3 and D4 phases (Table 1). Hammer is 60 cm long. (a) Qtz, Ky, Pl and tourmaline vein, cutting the penetrative S2 schistosity and deformed by D4 (Larecc anticline, eastern flank; Swiss coordinates: 698'710 / 137'630 / 2160 m). (b) Qtz, Pl, Ky, And and Ms vein. This outcrop is in the SW-part of the study area, on western flank of the major Larecc anticline; its orientation compared with (a) demonstrates rotation of the pre-existing veins by folding (697'925 / 137'610 / 2160 m). More examples (photos and sketches) of aluminosilicate-bearing veins are available at http://larecc.geoloweb.ch/

sense of shearing. Garnet and plagioclase show prograde zonation. Garnet, kyanite, staurolite, plagioclase, biotite and muscovite show textural equilibrium with clear contacts. Rutile and ilmenite are found in all studied samples. Ilmenite is more common and forms millimetre-sized rods parallel to the main schistosity. Chlorite is only found as retrogression of biotite, garnet or staurolite.

Structure and petrography of the aluminosilicate-bearing quartz veins

The AbQ veins developed as tension gashes during D3, always cutting the main S2 schistosity at high angle. They are cm- to m-sized and relatively abundant through all the metasediments of the Alpe Larecc. Some veins form symmetric extensional fractures with the country rock foliation pinching towards the tips of the crack (Fig. 4a; 6a). They are also found as sigmoidal tension gashes (Fig. 4b) or along top-to-the-north shear bands cross-cutting either foliation-parallel quartz veins, or the surrounding metasediments (Fig. 4c). The AbQ veins are also often located in the neck of pinch-and-swell boudinage structures resulting from the stretching of older quartz veins parallel to the foliation (Figs. 4d; 6b). Sigmoidal and shear band veins (Figs. 4b–c; 5) reflect a top-to-the-north sense of shear, whilst the growth of kyanite parallel to S2 in some veins (Figs. 5a; 6c) indicates that the veins open perpendicular to S2. Sigmoidal shape of veins and deformed kyanite in the veins suggest shear deformation following vein opening, whereas non-sheared symmetric veins with randomly oriented kyanite suggest post-shear-deformation opening and crystallization. Multiple stages of opening in one deformation event may have occurred. Sigmoidal AbQ veins may present an early stage, where mineralization in the shear bands and in boudin necks shows syn-deformational crystallizations. The symmetric veins may have formed late. D4 affects all veins and orients them (Figs. 3; 5a). The geometry of the AbQ veins resembles foliation boudinage (Platt and Vissers, 1980; Lacassin, 1988). They occurred isolated in the metasediments, and typical *en-échelon* arrangement of veins has not been observed. The orientation of the veins perpendicular to S3 is consistent with a hydrofracturing model. No interconnection of veins nor network formation are observed, which suggests local origin of the fluid. In some cases, flanking folds (Passchier, 2001) have been observed on both sides of the vein, reflecting rotation during the progressive deformation.

The investigated AbQ veins in the metasediments are generally composed of quartz, plagioclase, kyanite, andalusite, muscovite, ± staurolite. Among these minerals, only andalusite is not found in the host rock. In mica-rich layers veining is generally more important and veins are richer in aluminosilicates or staurolite. D3 extensional fractures are also observed in the amphibolites and the granitic gneisses, with a more restricted mineralogical assemblage of quartz, plagioclase and micas. Aluminosilicates are extremely rare in such lithologies: only one extensional fracture composed mainly of kyanite, oriented perpendicularly to the schistosity, has been observed in a block of orthogneiss south of Pizzo di Medasc. Mineral assemblages in veins thus appear to be largely controlled by the mineralogy of the host rock. The mineralization of the AbQ veins in the metasediments shows large heterogeneities (Fig. 5), but is generally quartz-dominant. The majority of the veins is composed of 50–80 vol% quartz, 0–30% plagioclase, 5–20% aluminosilicates, 0–10% muscovite and 0–5% staurolite. Veins show typically sections composed of quartz, plagioclase, or a mixture of mica and kyanite (Fig. 5). Quartz and plagioclase crystallize either in centimetre-sized aggregates, or form idiomorphic grains up to 10 cm in size. Isolated aluminosilicates may occur in large quartz aggregates. Such samples have been preferentially selected for oxygen isotope thermometry, to avoid cooling reequilibration during metamorphism (Putliz et al., 2002). Plagioclase is found in association with quartz and with aluminosilicates ± muscovite ± quartz. No significant compositional differences are observed for plagioclase from vein or host rock, except for sample L130 (An_{33} versus An_{12} to An_{22} for other plagioclase analyses in veins; Table 2). This is in agreement with the hypothesis of local origin for the material forming AbQ veins. Moreover, in contrary to zoned plagioclase from the host rock, plagioclase in veins never shows significant chemical zonation, but its composition is similar to the highest anorthite content found in the host rock.

Kyanite or/and andalusite are only occasionally predominant in shear bands or in the neck of quartz boudins, but form generally 0–20 vol% of the veins. Kyanite is most common and forms euhedral prismatic crystals up to 20 cm long. In some veins, the crystals are parallel to the N–S oriented mineral lineation in the host rock (Fig. 6c), indicating progressive growth during opening of the vein. However, in other cases, kyanite is randomly oriented (Fig. 6d), suggesting growth without significant deviatoric stress. Kyanite microprobe analyses (Table 2) from host rock or veins do not show significant differences, with 0.05 to 0.25 wt% Fe_2O_3 and insignificant amounts of TiO_2 (< 0.02 wt%) or MgO (< 0.03 wt%).

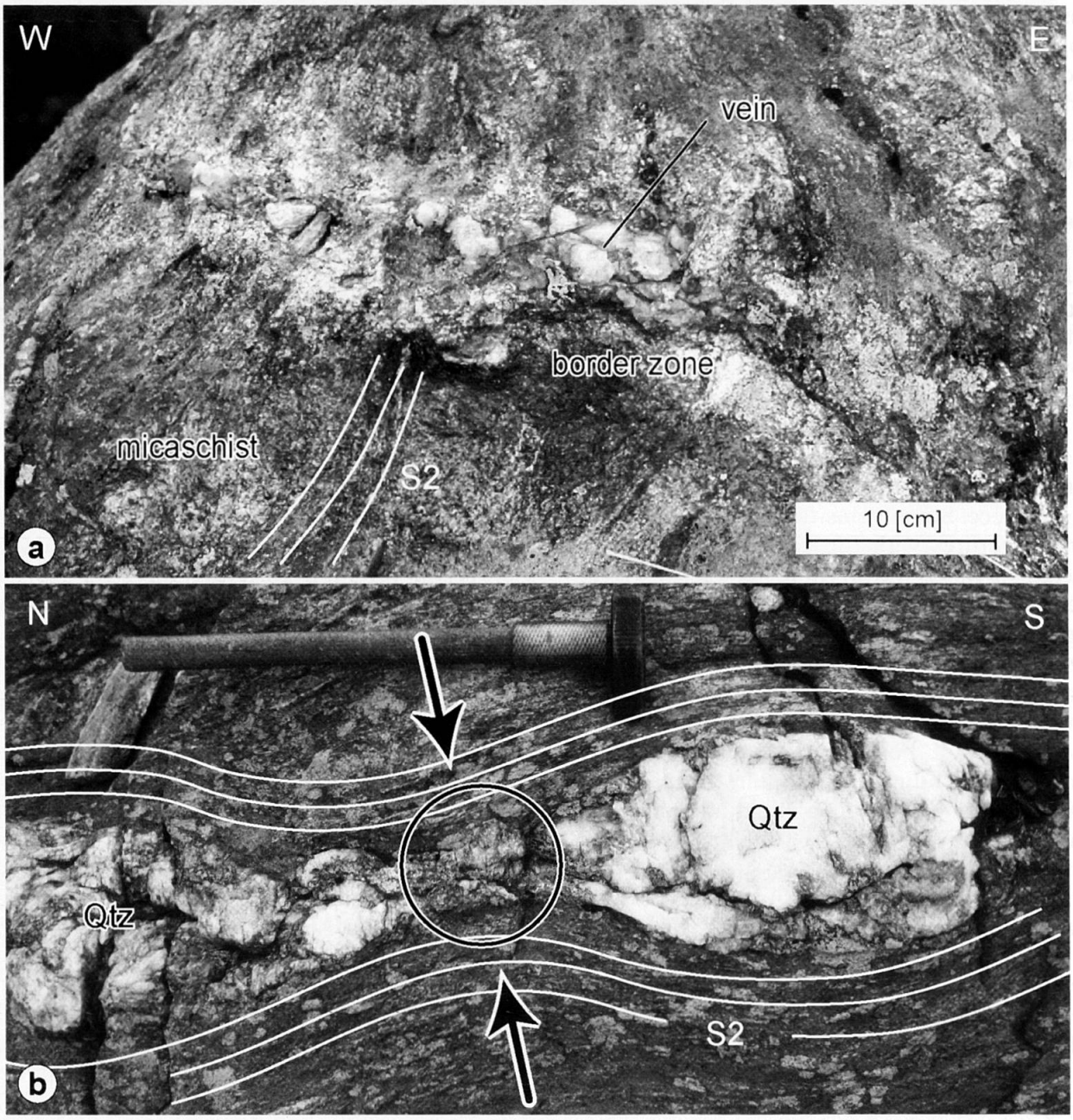

Fig. 6 (a) AbQ vein in micaschist, cutting the main schistosity S2 (Swiss coordinates: 138'130 / 697'880 / 1720 m). (b) AbQ vein in the boudin neck of an older Qtz vein, and showing horizontal N–S extension (Fig. 4d). Black arrows indicate bending of S2 foliation. Aluminosilicates are in the black circle, accompanied by Pl, Qtz and micas. Hammer is 60 cm long (Swiss coordinates: 137'635 / 698'710 / 2160 m).

Kyanite in the veins often presents a bluish core, which is never the case in the host rock, where crystals are always colourless.

In contrast to kyanite, andalusite is restricted to the veins. It generally forms centimetre-sized porphyroblast often enclosing relics of partially resorbed and sometimes slightly deformed kyanite (Fig. 6 e–g). This texture suggests crystallization of andalusite replacing kyanite, confirming the observation of Keller (1968) and Kerrick (1988). Kerrick (1988) argues that the kyanite to andalusite reaction was a volume-for-volume replacement reaction. The observed texture confirms that the volume increase due to crystallization of andalusite was minimal. Andalusite can form in the middle of undeformed aggregates of fan-shaped kyanite (Fig. 6d) or partially replacing a single kyanite enclosed in quartz aggregate under conservation of the original shape (Fig. 6g). No textural evidence suggesting new growth of andalusite catalysed at kyanite-fluid interface has been observed, such as rimming of andalusite around kyanite or andalusite adjacent to fractures within kyanite, confirming the observations of Kerrick (1988). Thus, retrograde reaction seams the most likely origin of the andalusite, rather than a new crystallization of aluminosilicate in the vein at lower metamorphic condition in the retro-

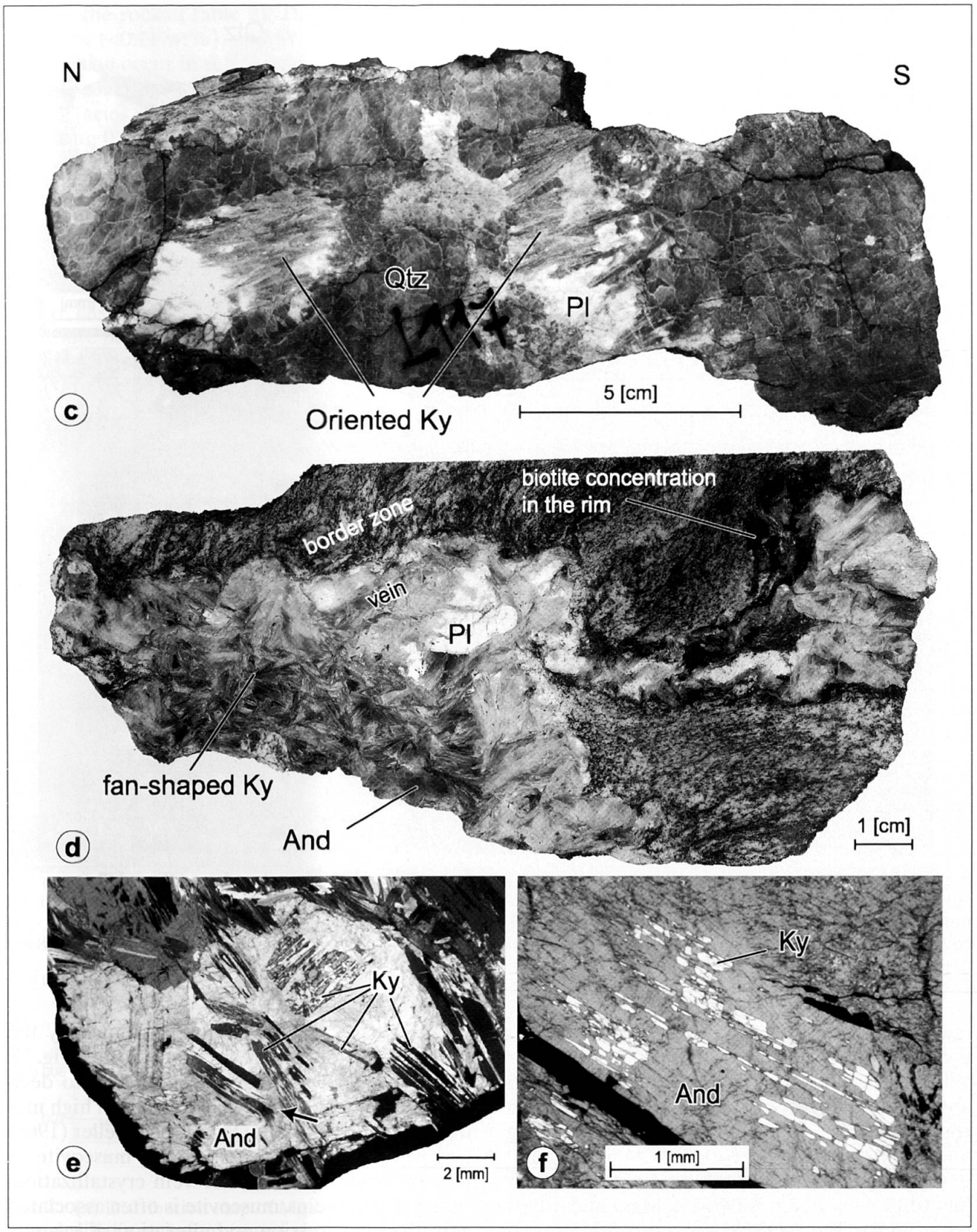

Fig. 6 (continued) (c) AbQ vein with Ky porphyroblasts oriented parallel to the penetrative schistosity and N–S oriented mineral lineation observed in the host rock. This texture indicates some of the AbQ veins formed by progressive opening during N-directed shearing (138'240 / 697'950 / 1725 m). (d) AbQ vein with fan-shaped Ky and And. Note the border zone of the vein formed by Bt and Pl (138'720 / 698'390 / 2235m). (e,f) Crossed-polarised microphotograph of And porphyroblasts containing inclusions of randomly oriented and partially resorbed prismatic Ky. This textural relation indicates And growth at the expense of Ky by a polymorphic reaction. Ky inclusions are sometimes deformed (black arrow in (e)), which is never the case for And (Swiss coordinates, e: 137'405 / 699'670 / 2350m; f: 137'430 / 697'855 / 2010m).

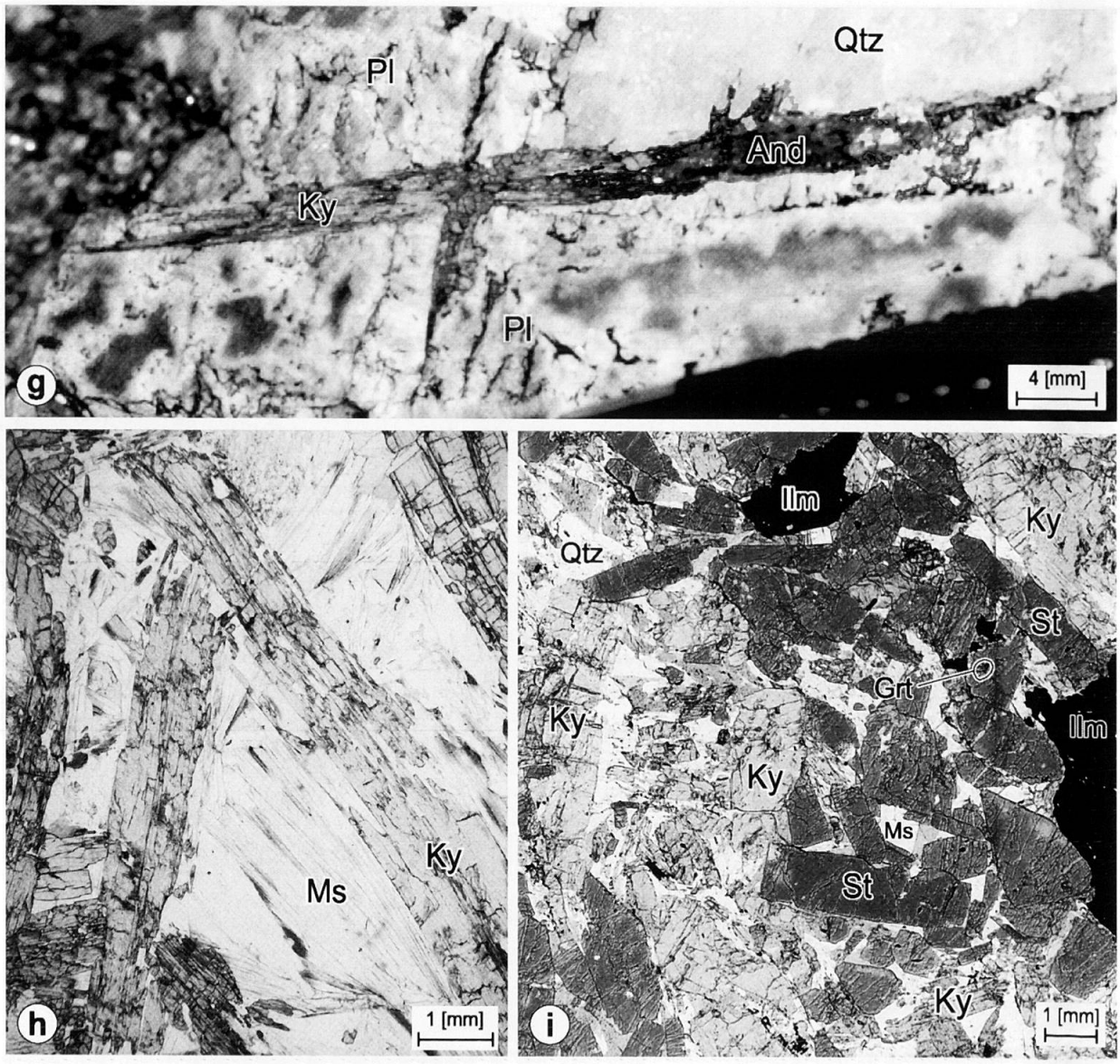

Fig. 6 (continued) (g) Large Ky rod (cm-sized), partially retrogressed into And, enclosed in a Qtz and Pl aggregate. (h) Plane-polarized light microphotograph of the core of an AbQ vein, with sheaf-like Ms in equilibrium with the non-oriented Ky grains (138'720 / 698'390 / 2235m). (i) Plane-polarized microphotograph of the core of an AbQ vein composed of St, Ky, Qtz, Ms, ± Ilm. Grt can be included in St, as a relic mineral of the host rock (137'790 / 698'840 / 2195m). All these and some additional pictures are available in colour on http://larecc.geoloweb.ch/

grade path. Representative average analyses andalusite border and core composition from four vein samples are given in Table 2. Similar to kyanite, andalusite is sometimes colour-zoned with a rose-coloured core due to enrichment in Fe^{3+}, Mg and Ti (up to 1.17 wt% Fe_2O_3, 0.39 wt% MgO and 0.08 wt% TiO_2). Crystal rims are generally colourless (0.13 wt% Fe_2O_3, 0.04 wt% MgO and < 0.04 wt% TiO_2). The Mg-rich core of andalusite is clearly visible in Figure 7a and a few chemical analyses highlight concordant variations of Fe and Mg (Table 2, Fig. 7b); it displays three major steps, an irregular Fe-rich core (0.9 wt% Fe_2O_3), an intermediate zone (0.5–0.7 wt% Fe_2O_3) and a border of andalusite with constant lower Fe-content (0.2–0.3 wt% Fe_2O_3). In contrast, only traces of Mg are present in kyanite, as shown by the darker colour of these relics in andalusite (Fig. 7).

Muscovite locally forms centimetre- to decimetre-sized zones in the vein reaching a high modal percentage (ca. 50%; Fig. 5b, 6h). Keller (1968) and Kerrick (1990) described this muscovite as late, replacing kyanite, after vein crystallization. In the studied veins, muscovite is often associated with the retrogression and alteration of kyanite, but also forms centimetre-sized (up to 5 cm) fans, or sheets parallel to the c-axis of kyanite, showing equilibrium contact with kyanite (Fig. 6h). Such a texture suggests growth of muscovite contemporaneous with the vein opening. Muscovite from host rocks and veins show similar (K,Na)-content, but the Si content in the veins is slightly lower

than in the rocks (Table 2). The F content is always low (<0.11 wt%), and Cl was not detected. Sericite can occur in retrogression of kyanite, andalusite or plagioclase, probably during greenschists facies. These are typically smaller crystal (less than 0.1 mm) present on cleavage planes or rimming altered crystals.

Staurolite is less abundant in veins than aluminosilicates. Figure 6i shows a photomicrograph of a decimetric zone in the core of a vein consisting of porphyroblasts of staurolite and kyanite, with quartz and cm-sized grains of ilmenite. In this particular case the country rock contains cm-sized staurolite porphyroblasts in a muscovite-rich matrix (Fig. 2a; sample L060). When staurolite or kyanite are in the border of the veins, they show a poikiloblastic texture with inclusions of minerals inherited from the host rock (e.g., quartz, biotite, garnet, muscovite, ilmenite, rutile). The staurolite composition in host rock and vein is nearly identical (Table 2). In two vein samples, ZnO contents are up to 1.94 wt%.

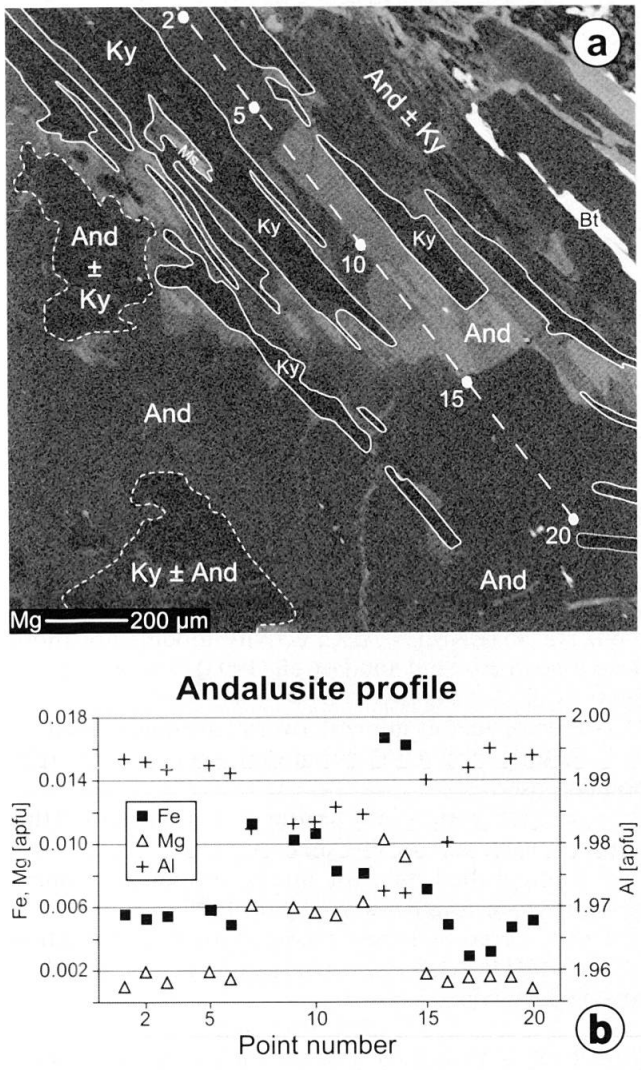

Fig. 7 (a) Distribution map of Mg for a cm-sized And crystal with Ky inclusions (sample L130). Analysis conditions: 15 kV, 20 nA, beam size = 2 µm, dwell time = 15 msec. As both Mg and Fe are correlated, this map indirectly represents also the zonation in Fe. The light-grey zone reveals the Fe-Mg-rich core of andalusite. Ky does not incorporate Mg and thus appears darker.
(b) Analytical profile (total length 1.7 mm). Complete averaged analysis of rim and centre points are given in Table 2.

Biotite occurs generally at the border of veins in micaschists containing staurolite porphyroblasts. Grains can be coarser than those in the host rock; crystals are oriented parallel to the border. The chemical composition of these biotites is similar to that of biotite in the host rock, with a slightly higher Al^{VI}-content in veins (Table 2). F and Cl are visibly more important in biotites than in muscovite, with up to 0.52 wt% and 0.05 wt%, respectively. Chlorite has been observed only as late retrogression of biotite in veins.

Accessory minerals in veins are ilmenite, rutile, tourmaline and apatite. Tourmaline can be an important constituent (Fig. 5a). Ilmenite is common, forming elongated plates or larger crystals reaching 2 cm. Rutile is rare and occurs together with ilmenite as inclusion in large staurolite or kyanite crystals, suggesting inheritance from host rock. However, in one plagioclase-dominated part of a vein, large idiomorphic rutile crystals (up to 2 mm) have been observed in and between grains, either isolated or in association with ilmenite. Garnet is also present at the borders of some veins, generally as inclusion in porphyroblasts (kyanite, plagioclase or staurolite; Fig. 6i). The restricted occurrence as inclusion and its rounded, corroded and sometimes broken texture suggest inheritance from host rock. The chemical range of a garnet from a biotite-rich border is $Alm_{77}Prp_{11}Sps_7Grs_5$ to $Alm_{78}Prp_{16}Sps_3Grs_3$ (sample L060 from core to border), comparable with garnet in the host rock (Table 2; Fig. 8).

Thermobarometry

Analytical and calculation procedures

The P–T conditions have been determined using multi-equilibrium thermobarometry on the diagnostic mineral assemblage. Four samples of Grt–St–Ky–Bt-bearing aluminous metasediments presenting well-equilibrated textures have been selected for analysis and PT-calculation (Tables 2; 3). All minerals have been analysed in a restricted zone of the thin section. Average compositions are calculated from at least three analyses of each phase in a sample (Table 2). In zoned minerals, an average is calculated using border points only, except if late reequilibration is signalised by an increase of Fe* ratio.

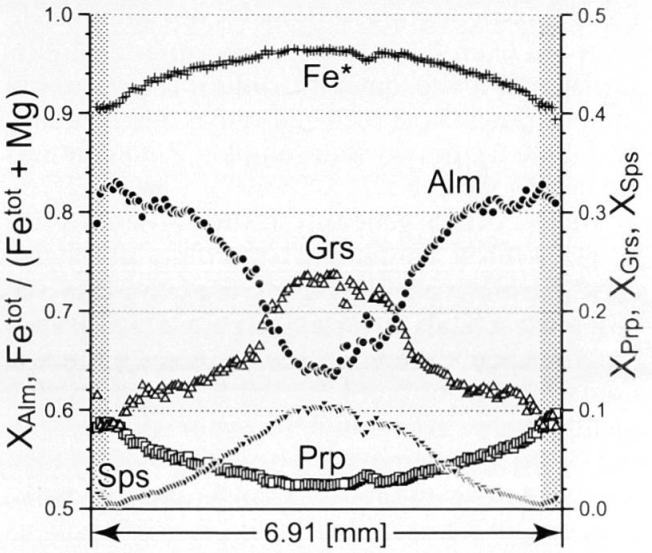

Fig. 8 Typical analytical transect of zoned garnet from metapelite (sample L005, 150 points) showing a continuous decrease in Fe^{tot}/Fe^{tot}+Mg ratio (Fe*), indicative of a constant increase in T (prograde zonation). A slight increase in Mn-content at the very border is indicative of resorption (grey bands). However, the Fe* ratio remains constant (or shows a slight decrease) in this border, indicative of constant (or a bit higher) T.

Two internally consistent thermodynamic databases have been used to quantify P–T conditions in the CNKFMASH + TiO_2 + MnO system: TWQ 2.02 (database BA96a.DAT, solution model BA96a.SLN, Berman, 1988; 1991; Berman and Aranovich, 1996; update January 1997) and THERMOCALC 3.21 (Powell and Holland, 1985; Holland and Powell, 1985; 1998; update February 2002). For THERMOCALC, activity models used are summarised in Holland and Powell (1998). Solid-solution models used in TWQ are listed in Table 3. Both THERMOCALC and TWQ involve subroutines that allow identification of end-members of solid-solution minerals that produce large errors on the PT estimates (generally due to a low or aberrant activity calculation). Such end-members may be ignored during the PT calculations by removing them from the pertinent thermodynamic database. For biotite, a four-end-member model is used in TWQ, comprising provisional properties of annite, phlogopite, eastonite and siderophyllite. Activity calculations take into account four end-members, but reactions inducing annite and eastonite have been removed, as they show an unacceptable large scatter in calculated reactions. The few percent of Ti in biotite, which is probably responsible of some vacancies on octahedral site (Dymek, 1983; Henry and Guidotti, 2002), may be problematic for both databases used: all Ti is included in octahedral site M2, together with Fe, Mg and Al^{VI}, but no Ti-biotite model is present in TWQ or THERMOCALC. This may slightly underestimate annite-phlogopite activities with the profit of siderophyllite-eastonite. Muscovite and paragonite end-

Table 3 Assemblage used for thermobarometric calculations on paragneiss (L005) and three micaschists.

Activity models used in TWQ		L005	L006	L013	L064
Fuhrman and Lindsley, 1988	Plagioclase	O	Z	O	Z
Berman and Aranovich, 1996	Garnet	Z	Z	R	R
Berman and Aranovich, 1997*	Biotite	O	O	O	O
Chatterjee and Froese, 1975	Muscovite	O	O	O	O
Not used in TWQ	Staurolite	O	O	O	O
Berman and Aranovich, 1996	Ilmenite	O	O	O	O
	pures EM	Qtz, Rt, Ky	Qtz, Rt, Ky	Qtz, Rt, Ky	Qtz, Rt, Ky

THERMOCALC	EM excluded	pa geik	pa	pa spss	pa geik
	LIR	9	10	9	9
	aH_2O	0.94	0.83	0.76	1.00
	T [°C]	**620**	**635**	**623**	**636**
	incert. [°C]	26	21	20	21
	P [kb]	**8.4**	**7.7**	**8.5**	**8.3**
	incert. [kb]	1.0	0.9	0.9	0.8
	Corr. fact.	0.090	0.118	0.119	0.121
	Fit	1.25/1.42	0.62/1.39	0.54/1.42	0.85/1.42
TWQ	LIR	5	5	5	5
	xH_2O	0.27	0.36	0.27	0.36
	T [°C]	**586**	**618**	**599**	**596**
	incert. [°C]	12	7	16	19
	P [kb]	**8.7**	**8.6**	**9.2**	**8.3**
	incert. [kb]	0.4	0.2	0.5	0.5

Two different but internally consistent databases have been used, THERMOCALC 3.21 and TWQ 2.02 (BA96a.DAT and. SLN). Activity models for the solid solutions used in TWQ are listed in the upper left column. For THERMOCALC, activity models are those described in Holland and Powell (1998). See text for details.

O — Homogeneous mineral, overall average is used

Z — Zoning in mineral (prograde), average on border points is used

R — Zoning with a late border re-equilibration (this border is excluded for P–T analysis)

* — Unpublished data for biotite properties (annite, phlogopite, eastonite, siderophyllite)

EM excl. = End-members excluded for P-T calculation in THERMOCALC (pa = paragonite, geik = geikelite, spss = spessartine)

LIR — Linear Independent Reaction

Corr. fact. — Correlation factor for construction of ellipse of uncertainty

Fit — Factor of fit for THERMOCALC results

aH_2O — estimated activity of water by THERMOCALC

xH_2O — estimated mole fraction of water by TWQ.

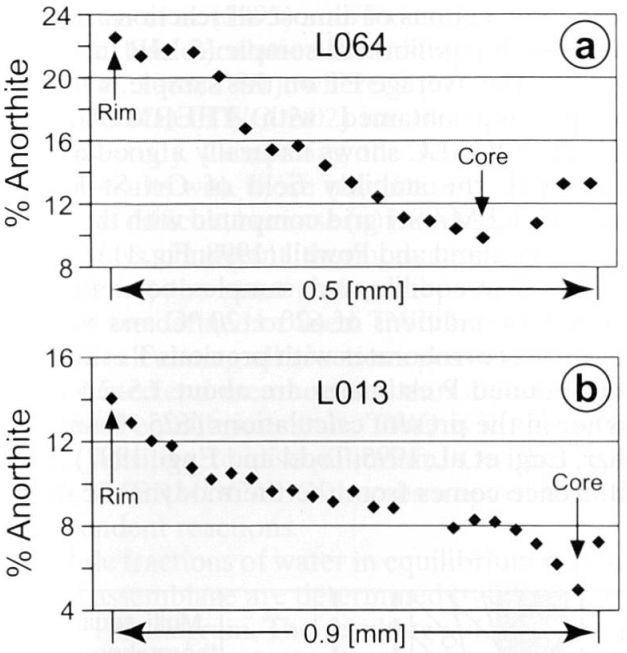

Fig. 9 Analytical transect of Pl in two micaschist samples with porphyroblasts of Grt, Ky and St.
(a) Samples L064 and (b) L013 are both used for thermobarometry and border points have been taken for P–T calculation. As in zoned Grt, the anorthite-content in Pl increases regularly, consistent with a continuous increase in T (prograde zoning).

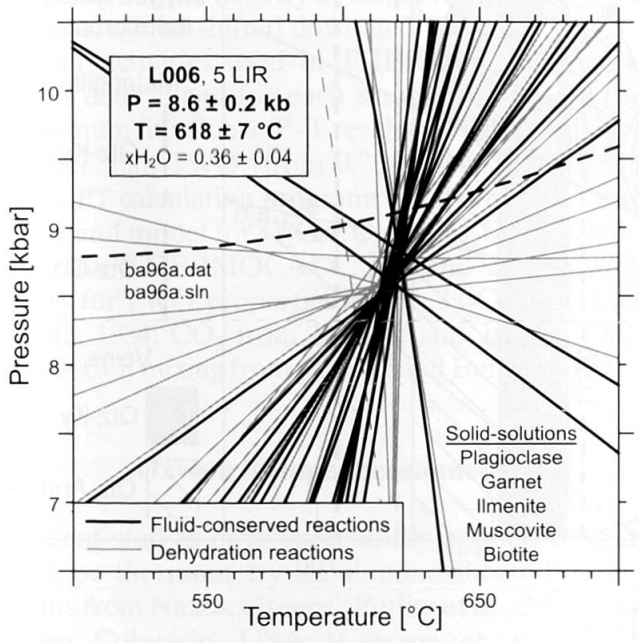

Fig. 10 TWQ result for metapelite sample L006. In this result, equilibrium is well achieved, as all reactions involving alm, prp, grs, siderophyllite, phl, ms, pg, ab, an, ilm, Rt, Ky and Qtz cross-cut in the same P–T region. Mole fraction of water in equilibrium with selected assemblage has been calculated in a T–xH_2O diagram for a pressure of 8.7 kbar. Dashed lines are equilibria situated more than 1.5 σ outside P–T average presented in Table 3.

members of white micas are considered in TWQ, but in THERMOCALC only muscovite and celadonite are used, paragonite being always withdrawn, due to low activity calculated. Spessartine component of garnet has been sometimes excluded in average-PT calculated by THERMOCALC (Table 3, sample L013), whilst it was never a part of the TWQ 2.02 database. Andradite has not been considered and in a general way Fe^{3+} is not considered in the calculations. This has little influence on results: using a maximum Fe^{3+} content of 4% for garnet (determined by charge balance) and 10% for biotite (Guidotti and Dyar, 1991; Dyar et al., 2002) shift results by approximately 10 degrees and 0.1 kbar down, which is insignificant as total uncertainties are at least three times higher. For plagioclase, anorthite and albite are always considered. For staurolite an ideal solution model has been used in THERMOCALC, but was not considered in TWQ. Pyrophanite is not defined in TWQ and geikelite activity is always insignificant. In THERMOCALC, these two end-members are also often ignored, due to low activity calculation (Table 3).

Metamorphic assemblages

Selected metapelite rock assemblages (Table 2; Fig. 2a) indicate equilibration under amphibolite-facies conditions in the kyanite-staurolite zone (Frey and Ferreiro-Mählmann, 1999; Table 3). In an AFM diagram, the whole-rock analyses from two samples (L013 and L064) plot on the St–Bt join, consistent with a four-phase equilibrium Grt–St–Ky–Bt. The diagnostic peak equilibrium assemblage in micaschists and paragneisses consist of Ky + St + Grt + Bt + Ms + Pl + Qtz, with accessory Ilm and Rt. Garnet and plagioclase zoning patterns reflect a continuous increase in T during porphyroblast growth. This is indicated by a regular decrease in Fe* ratio from core to rim in Alm-rich garnet in metapelites. Some garnet rims show an increased Sps-component suggesting resorption (Fig. 8). However, these rims are probably in equilibrium with the matrix, especially with biotite, which is often found in P shadows of garnet. Plagioclase zoning patterns also reflect a T increase during growth, which is reflected by an increase in anorthite content from 8% in the core to 22% at the rim in aluminous metasediments (Fig. 9). Only samples L013 and L064 may have suffered reequilibration at lower T, possibly with biotite or staurolite, suggested by an increase in Fe* ratio at the rim of the mineral. In such case, the lowest Fe* ratio has been taken, in order to obtain the maximum T recorded. Resorption marked by an increase in Mn-content at the rim may occur

during prograde or retrograde path. However, this increase is not correlated with an increase in Fe*, suggesting a reequilibration near the peak of metamorphism in garnet of sample L005 (Fig. 8).

P–T results

Multi-equilibrium thermobarometric results are presented in Table 3. Results of THERMOCALC involve more than 8 linearly independent reactions (LIR) and are well constrained at 620–635 °C and 7.7–9.0 kbar (23 to 27 km). For results from TWQ, slightly lower T (580–620 °C) but similar P (8.3–9.2 kbar) are estimated. The best TWQ result is obtained on sample L006, as reflected by close intersections of almost all reactions, indicative of well equilibrated sample (5 LIR in TWQ, Fig. 10). The average PT on this sample is similar to the one obtained with THERMOCALC. THERMOCALC shows naturally a good agreement with the stability field of Grt–St–Ky–Bt from the KFMASH grid computed with the database of Holland and Powell (1998; Fig. 11).

The best-equilibrated samples converge towards PT-conditions of 620 ± 20 °C and 8.5 ± 1 kbar. This corroborates with previous T estimates but obtained P estimates are about 1.5–2.5 kbar higher in the present calculations (625 °C and 6.5 kbar, Engi et al., 1995; Todd and Engi, 1997). This difference comes from the thermodynamic data-

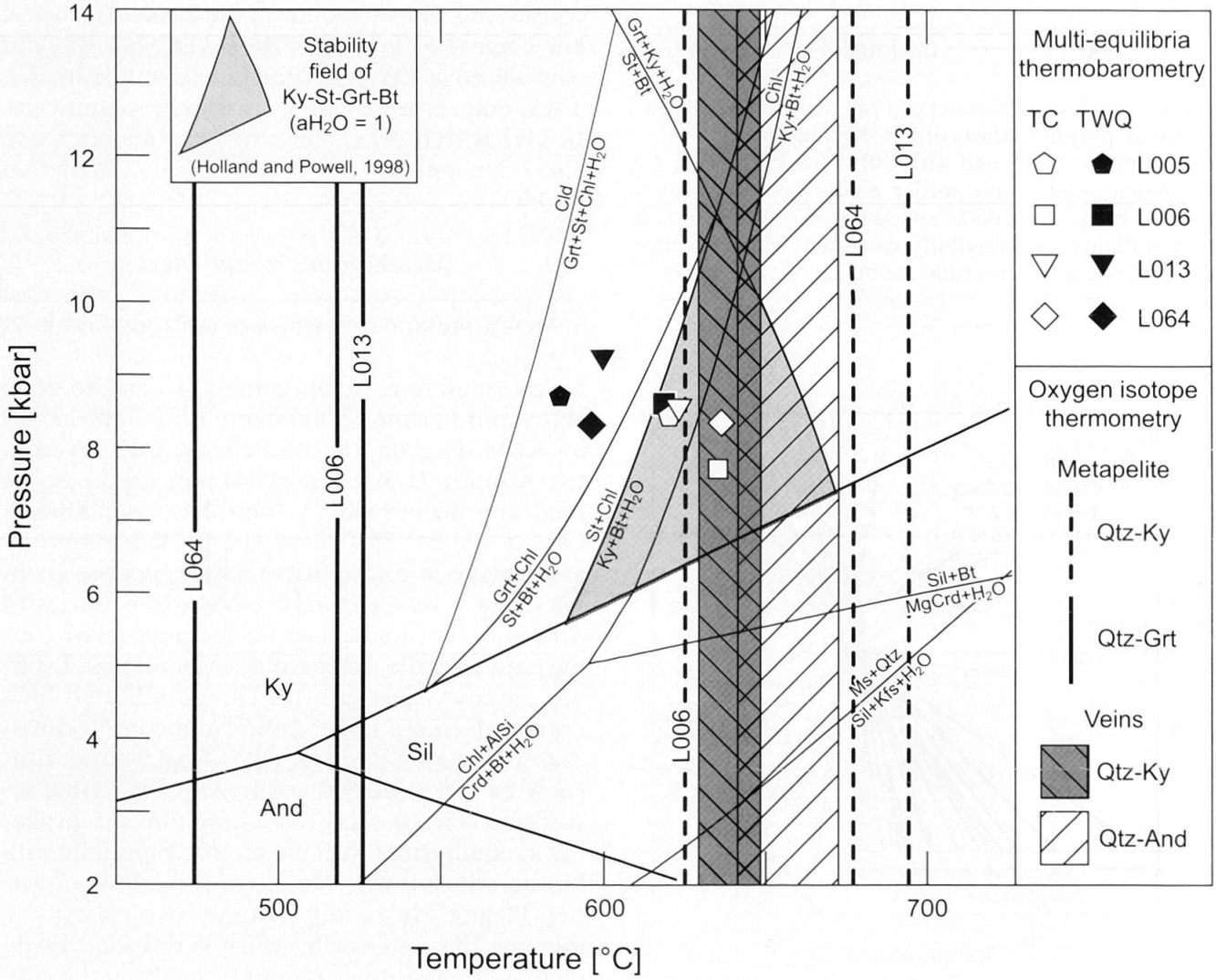

Fig. 11 Thermobarometric conditions calculated for micaschists (L006, L013 and L064) and paragneiss (L005) samples, by the use of TWQ and THERMOCALC (=TC). P–T average used here calculated including fluid-involving reactions. These results are the same as in fluid-conserved reaction calculations. Sample L006 represents the best-equilibrated sample with TWQ and THERMOCALC. Oxygen isotope thermometry on Qtz-aluminosilicates and Qtz–Grt from veins and host-rocks is also presented (see text). Errors not represented (see Tables 3, 4). In the background, some selected reactions from the KFMASH grid (at $xH_2O=1$) of metapelites constructed with database of Holland and Powell (1998). Complete P–T grid available at http://ees2.geo.rpi.edu/MetaPetaRen/GibbsWeb/Gibbs_Grids.html. Considering a lower water activity, dehydration reactions will be shifted to lower T (min. 50 °C lower at $xH_2O=0.3$).

base. Engi et al. (1995) and Todd and Engi (1997) used for their calculation the first version of TWQ (Berman, 1988; 1991), whereas the updated version of TWQ (TWQ 2.02) has been used in the present study. Comparing the relevancy of the TWQ results with those obtained by THERMOCALC is difficult, because (a) both use a different but always consistent thermodynamic database, and (b) not the same end-members and activity models are defined or used. TWQ has the advantage of calculating all reactions possible between the selected end-members and thus allows examination of equilibrium state. TWQ is in this sense more sensitive to disequilibrium. On the other hand, THERMOCALC chooses a set of linearly independent reactions.

Mole fractions of water in equilibrium with selected assemblage are determined by TWQ using a T–xH_2O diagram. The resulting values are very low (0.27 to 0.36 xH_2O), but comparable values have been obtained with TWQ 2.02 on similar samples coming from Alpe Sponda, 10 km more to the east (600 °C, 7 kb, 0.3 xH_2O; Chollet, 2000). The TWQ results are inconsistent with reactions plotted in the background of Fig. 11, as we would expect them to fall in the Grt–St–Ky–Bt field. However, these reactions belong to the KFMASH grid calculated for a water activity of 1 and with the Holland and Powell database. Considering a water activity of 0.3, devolatilization reactions will be shifted down in T by at least 50 °C. Water activities used in THERMOCALC have been determined for each sample by finding the minimum fit value in P–T results. Activity is always higher than TWQ (from 0.76 to 1.00 aH_2O), but both PT calculation programs use a different database and model for H_2O, CO_2 and H_2O–CO_2 mixing (for THERMOCALC, Holland and Powell, 1998; for TWQ, properties of pure H_2O from Haar et al., 1984; CO_2 from Kerrick and Jacobs, 1981; H_2O–CO_2 mixing from Maeder and Berman, 1991).

Oxygen isotope thermometry

Recent studies have successfully applied oxygen isotope thermometry on aluminosilicate-bearing veins from Naxos, Greece (Putlitz et al., 2002) and from Colorado, USA (Cavosie et al., 2002). Agreement between results of oxygen isotope thermometry and conventional thermobarometry shows that such veins record high-T oxygen-fractionation. In order to correlate the formation of the veins with the established metamorphic history we have applied oxygen isotope thermometry on Qtz-aluminosilicate pairs from veins and host rocks. Host rocks samples have generally not been taken in direct contact to the veins. However, samples L006 and L064 have been taken in the neighbourhood of samples L038, L005, L124 and L050, L119 respectively (Fig. 2a).

Five AbQ veins containing kyanite and andalusite have been selected for oxygen isotope thermometry. The $\delta^{18}O/^{16}O$ isotopic ratios of all minerals of each sample were measured twice in one day and the reproducibility was generally better than 0.1‰. To correlate the isotopic results to the thermobarometric results, kyanite, quartz and garnet separates from three country rock micaschists were analysed to determine equilibration temperatures for Qtz–Grt and Qtz–Ky pairs. Samples have been crushed and sieved for mineral separation. Considering the grain size of the pertinent minerals in thin section, a fraction between 250 and 500 μm was chosen for host rocks and tension gashes. After shaking-table and magnetic separation, careful handpicking allowed selection of the purest minerals. Quartz, kyanite and garnet separates from host rock samples L013 and L064 were leached with HF 10% for 10 to 12 hours at room T to remove impurities and surface contaminations of mica and plagioclase. Sample batches of 1.5–2.5 mg were analysed by laser fluorination (Sharp, 1992) at the Stable Isotope Laboratory of the University of Lausanne. Analyses have been reported relative to Standard Mean Ocean Water (SMOW) and corrected using an in-house standard (Qtz Lausanne-1: $\delta^{18}O_{SMOW}$ = 18.15‰) and the international standards NBS-28 ($\delta^{18}O_{SMOW}$ = 9.6‰) and Grt UWG-2 ($\delta^{18}O_{SMOW}$ = 5.85‰). Each run was bracketed by standard analyses at start and finish to allow corrections of constant and systematic errors. The temperatures are determined with the following relation

$$\delta^{18}O_{x-y} \approx 10^3 \ln[\alpha(x-y)] = a_{xy} \times 10^6/T,$$

where $10^3\ln[\alpha(x-y)]$ is the fractionation between the two minerals x and y ($\approx \delta^{18}O_{x-y}$) and T is in K. Values of the fractionation coefficients a_{xy} are from the calibration of Sharp (1995; $a_{Qtz-Ky} = a_{Qtz-And} = 2.25 \pm 0.2$ and $a_{Qtz-Grt} = 3.1 \pm 0.2$), which yield T-estimates that are in agreement with phase equilibrium thermometry on middle to upper amphibolite-facies rocks (Moecher and Sharp, 1999; Vannay et al., 1999; Putlitz et al., 2002; Cavosie et al. 2002).

During cooling, isotopic composition of minerals can be modified because of diffusion between the different phases present (Giletti, 1986), which leads to oxygen isotope re-equilibration. Of the analysed phases in this study, quartz is most easily affected by diffusional re-equilibration (Giletti, 1986; Eiler et al., 1993), which would lead to an erroneous T-estimate. However, AbQ veins analysed are coarse-grained, and therefore less likely

Table 4 $\delta^{18}O_{SMOW}$ values of (a) Ky, And and Qtz from AbQ veins and (b) Ky, Qtz and Grt in host rock. All values have been corrected to Garnet UWG-2 or Quartz Lausanne-1 standards. Values of $\delta^{18}O$ in the five first columns are given in ‰. T calculated according to Sharp (1995).

a

		Standard-corrected $\delta^{18}O_{SMOW}$			$\delta^{18}O_{A-B}$		Temperature [°C]	
		$\delta^{18}O$ (Qtz)	$\delta^{18}O$ (Ky)	$\delta^{18}O$ (And)	Qtz-Ky	Qtz-And	Qtz-Ky	Qtz-And
VEINS	L005	*9.41*	*6.62*	*6.74*	*2.76*	*2.64*		
		9.29	*6.72*	*6.77*	*2.54*	*2.49*		
	avg	9.35 ± 0.08	6.67 ± 0.07	6.76 ± 0.02	2.65 ± 0.08	2.57 ± 0.08	**650** ± 30	**665** ± 30
	L038	*11.77*	*8.98*	*9.22*	*2.76*	*2.52*		
		11.71	*8.92*	*9.12*	*2.77*	*2.56*		
	avg	11.74 ± 0.04	8.95 ± 0.05	9.17 ± 0.07	2.76 ± 0.02	2.54 ± 0.02	**630** ± 25	**670** ± 25
	L050	*9.22*	*6.00*	*6.74*	*3.20*	*2.47*		
		9.57	*7.40*	*6.63*	*2.15*	*2.92*		
	avg	9.40 ± 0.24	6.70 ± 0.99	6.68 ± 0.08	2.68 ± 0.72	2.69 ± 0.18	**645** ± 250	**640** ± 60
	L119	*9.57*	*6.66*	*7.04*	*2.88*	*2.50*		
		9.54	*7.07*	*6.98*	*2.45*	*2.53*		
	avg	9.55 ± 0.02	6.86 ± 0.29	7.01 ± 0.04	2.67 ± 0.21	2.52 ± 0.07	**645** ± 75	**670** ± 25
	L124	*8.75*	*6.38*	*6.52*	*2.35*	*2.21*		
		8.63	*6.41*	*6.61*	*2.21*	*2.01*		
	avg	8.69 ± 0.08	6.39 ± 0.02	6.57 ± 0.07	2.28 ± 0.08	2.11 ± 0.08	**720** ± 35	**760** ± 40

b

		Standard-corrected $\delta^{18}O_{SMOW}$			$\delta^{18}O_{A-B}$		Temperature [°C]	
		$\delta^{18}O$ (Qtz)	$\delta^{18}O$ (Ky)	$\delta^{18}O$ (Grt)	Qtz-Ky	Qtz-Grt	Qtz-Ky	Qtz-Grt
METAPELITES	L006	*14.19*	*11.47*	*9.73*	*2.69*	*4.41*		
		14.57	*11.61*	*9.30*	*2.92*	*5.21*		
	avg	14.38 ± 0.08	11.54 ± 0.07	9.52 ± 0.02	2.80 ± 0.09	4.81 ± 0.22	**625** ± 25	**530** ± 35
	L013	*9.47*	*6.95*	*4.54*	*2.50*	*4.90*		
		9.56	*7.22*	*4.70*	*2.32*	*4.83*		
	avg	9.52 ± 0.08	7.09 ± 0.07	4.62 ± 0.02	2.41 ± 0.14	4.86 ± 0.09	**695** ± 55	**525** ± 15
	L064	*9.98*	*7.50*	*4.43*	*2.46*	*5.51*		
		9.94	*7.40*	*4.30*	*2.52*	*5.60*		
	avg	9.96 ± 0.08	7.45 ± 0.07	4.37 ± 0.02	2.49 ± 0.07	5.56 ± 0.08	**680** ± 25	**475** ± 10

to be affected by late diffusion. The veins analysed here have a high modal abundance of quartz, which will be an important isotopic reservoir in the system where the exchanges take place and its $\delta^{18}O$ isotopic value will not change during cooling (Putlitz et al., 2002). The $\delta^{18}O_{smow}$ values of the minerals in the AbQ veins and their host rocks are presented in Table 4, and the $\delta^{18}O_{Qtz}$ – $\delta^{18}O_{And/Ky}$ or $\delta^{18}O_{Qtz}$–$\delta^{18}O_{Grt}$ graphs are in Figure 12. The data reveal similar isotopic values for $\delta^{18}O_{Ky}$ and $\delta^{18}O_{And}$ in each vein, which indicates that oxygen was not fractionated between the two polymorphs. The isotopic ratios of the veins and their host rocks are also similar, which is consistent with local mobilization of the metamorphic fluids, in agreement with our petrographic observations and previous work (Kerrick, 1990). The isotopic ratios of Alpe Larecc are similar to those reported from Alpe Sponda, a few kilometres away, but also part of the Campo Tencia metasediments (Hoernes and Friedrichsen, 1980; Fig. 12a). Isotopic ratios of the only kyanite vein analysed at Alpe Sponda, as well as the ratios of its host rock indicate equilibration at a significantly lower T, which suggests that these samples were affected by diffusion during cooling (Hoernes and Friedrichsen, 1980).

The temperatures obtained with Qtz–Ky pairs from the AbQ veins vary between 600 and 675 °C (Table 4, Fig. 13). The same pair from the host metapelites yields similar temperatures between 600 and 700 °C, in agreement with those obtained

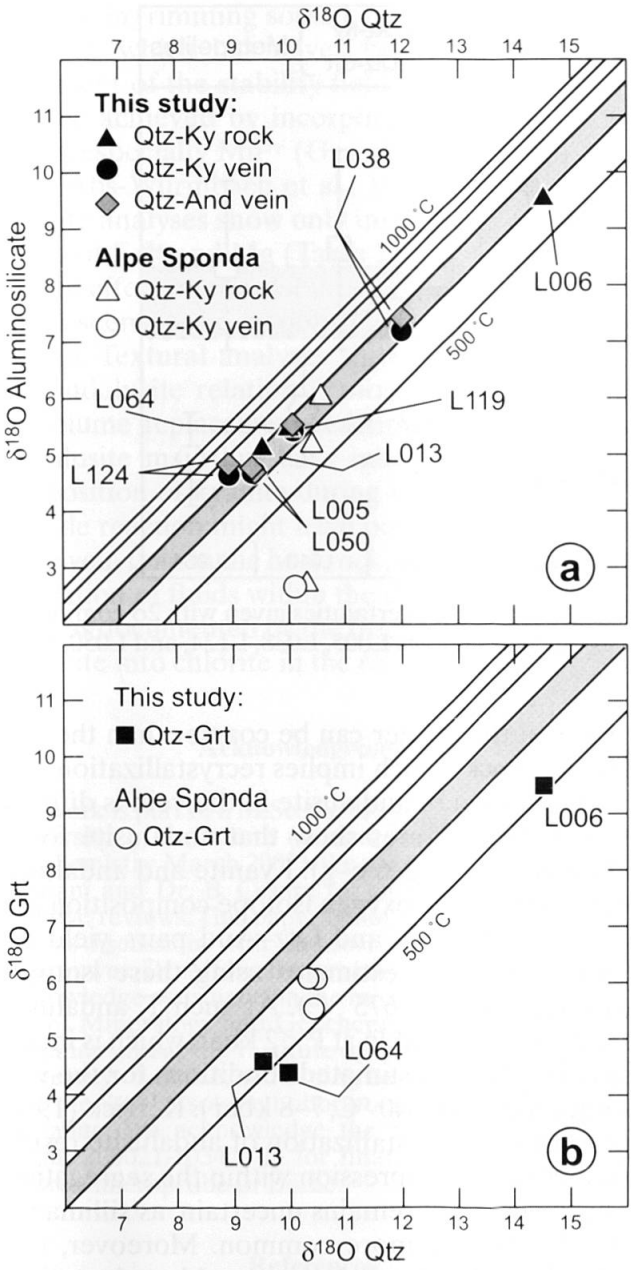

Fig. 12 (a) Diagrams $\delta^{18}O_{aluminosilicate} - \delta^{18}O_{Qtz}$ and (b) $\delta^{18}O_{Grt} - \delta^{18}O_{Qtz}$ for the AbQ veins and some host rock. Errors not represented here (see Table 4). Grey band in both graphs is T stability field of Ky–St–Grt–Bt.

by multi-equilibrium thermobarometry on the same samples (Fig. 11). This supports the inference that the AbQ veins formed during the peak of the metamorphism. The T range obtained for host rock minerals is larger than for the veins, which may reflect the smaller grain size of the metapelites and their consequent higher susceptibility for late diffusion.

Garnet–quartz pairs from the metapelites yield temperatures between 470 and 530 °C, systematically about 100 °C below those of the Qtz–Ky pairs, which indicates that Grt is not in isotopic equilibrium with quartz and kyanite. Because of very slow oxygen diffusion in garnet, it is likely to preserve the isotopic value characteristics of its crystallization conditions. Petrographic observations and garnet major element zoning (Fig. 8) indicate continuous prograde garnet growth, which may also have produced isotopic growth zoning (Chamberlain and Conrad, 1991). In that case the measured $\delta^{18}O$ would reflect an average of an evolution of isotopic composition (Vannay et al., 1999).

Discussion on the formation of the aluminosilicate–bearing quartz veins

The AbQ veins are isolated extensional fractures resembling foliation boudins (Platt and Vissers, 1980; Lacassin, 1988), directly related to a top-to-the-north shearing. They are contemporaneous to the regional D3 phase of deformation, coeval with the metamorphic peak conditions in amphibolite facies in the stability field of garnet, staurolite, kyanite and biotite. Formation of such veins near peak conditions, when the accumulation of the fluids generated by devolatilization reach the maximum, are found elsewhere. On Naxos, for example, aluminosilicate veins also recorded the regional peak in the Ky–Sil zone between 620 and 700 °C (Putlitz et al., 2002), whereas in Colorado, segregations recorded oxygen isotope equilibration temperatures between 600 °C and 650 °C, in agreement with the cation-exchange thermometry for the host rock (Cavosie et al., 2002). To allow such isolated fracturing in the ductile regime, a high P_{fluid} is required to displace the Mohr circle into the domain of tensile fracturing. Devolatilization reactions are capable of generating substantial fluid overpressure (Connolly, 1997): for example, the reaction Chl + Ms = Bt + Qtz + Ky/St + H_2O (Connolly, 1997; Kerrick, 1988) can produce kyanite or staurolite and may be an important source for the vein-forming fluid. The analogy between the mineralogy in the vein and the host rock, the similar isotopic composition of quartz and kyanite in veins and host rocks, and the isolated occurrence of the veins suggest local origin of the fluid. A schematic model of AbQ-vein formation is shown in Figure 14. The vein opening induces local drop of *P* inside the crack, which generates a gradient between pores of the host rock and the crack and gives rise to the migration of the fluid into the open cavity (Etheridge et al., 1984). The *P* gradient is limited to the direct border to the host rock, as P_{fluid} in the crack should always remain equal to σ_3 in order to avoid closing of the crack. A reaction occurs between the migrating fluid and the host rock, inducing a depletion halo around the vein. This zone is marked by enrichment of biotite and depletion in

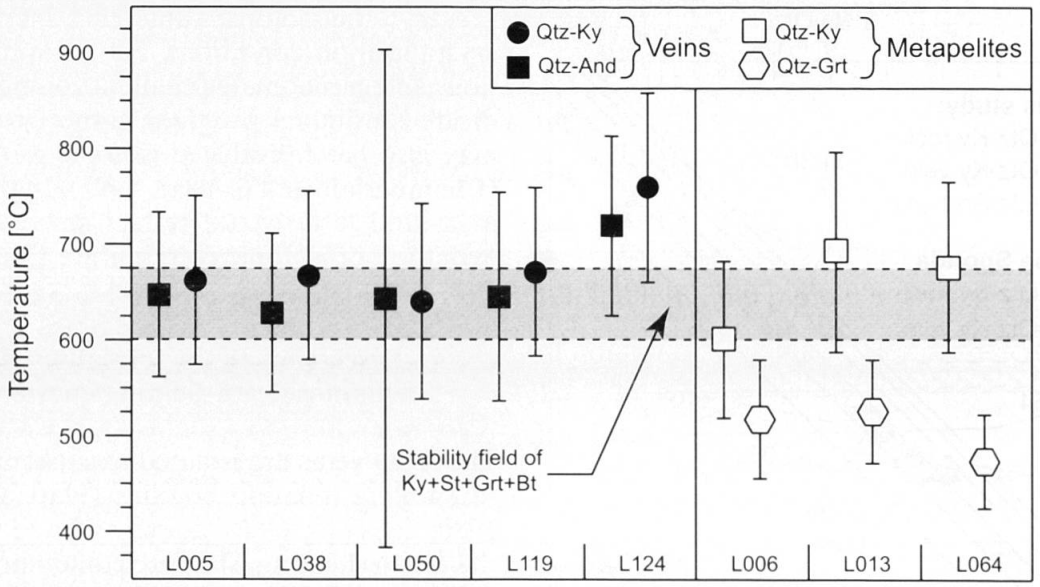

Fig. 13 Thermometry by the oxygen isotope on AbQ veins and host rocks. Uncertainties given with 2σ confidence. Rock samples L006 and L064 are situated in the same region as the vein samples L005, L038, L124, and L050, L119.

quartz, muscovite, kyanite and, substantially, in plagioclase (Keller, 1968; Klein, 1976; and Kerrick 1988, Figure 14 stage c). A model of diffusive mass transfer through stagnant fluid may be applicable for the vein formation (Cesare, 1994; Widmer and Thompson, 2001), with fluid migration connected to the preferential dissolution of Si, Al, Na and K (Woodland and Walther, 1987; Walther and Woodland, 1993). The extremely low solubility of Al_2O_3 in aqueous fluids makes difficult to explain such diffusional origin of kyanite. Kerrick (1988; 1990) concluded that Al was most likely present in the fluid as an alkali-aluminium complex. Decomposition of muscovite in the border zone of the vein is considered to be the K-source in this fluid (Kerrick, 1988). To some extent, all the dissolved phases in the border zone of the vein reprecipitate in veins (Fig. 14, stage d). The biotite grains in the border can be coarser than those in the host rock, which implies recrystallization.

Formation of andalusite in the vein is difficult to explain. Textures show that andalusite forms after kyanite (Fig. 6 e–g). Kyanite and andalusite exhibit the same oxygen isotope composition and therefore, Qtz–Ky and Qtz–And pairs yield the same range of T estimates using these isotopes (around 600 and 675 °C). At such T, andalusite should only be stable at P < 2 kbar, which is inconsistent with the estimated conditions for the vein formation (600–640 °C; 7–8 kbar). Kerrick (1988) proposes that crystallization of andalusite results from local decompression within the segregation. This mechanism remains uncertain, as sillimanite should then be more common. Moreover, new crystallization of andalusite should preferentially occur in relation with a new crack or at the border

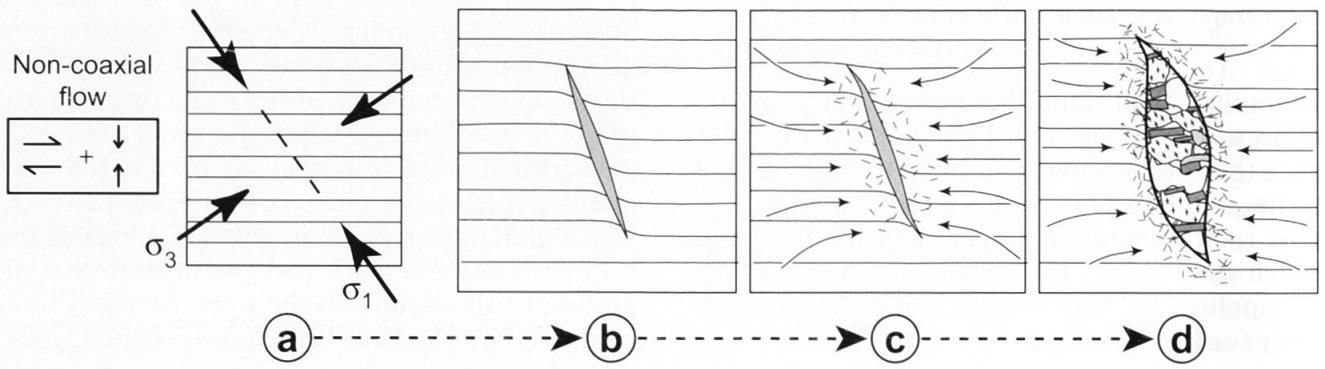

Fig. 14 Different stages of formation of the aluminosilicate tension gashes in a context of general shearing. σ_1, σ_3: maximal and minimal stress. When P_{fluid} is more important than the sum of tensile strength and minimal stress component, a crack can open (stages a and b). The opening yields a gradient in P, which leads to fluid migration. The fluids provoke a reaction with the host rock in the surrounding of the vein, giving rise to dissolution of alkaline and aluminous phases (stage c). The dissolved material will finally precipitate inside the vein (stage d). See text for further explanation (adapted from Etheridge, 1984; Kerrick, 1990).

of the vein, rimming some kyanite crystals or aggregates, which has never been observed. Enlargement of the stability field of aluminosilicate may be achieved by incorporation of other elements, especially Mn^{3+} (Grambling and Williams, 1985; Abs-Wurmbach et al., 1983). However, andalusite analyses show only insignificant incorporation of Fe^{3+} and Mg (Table 2), which has a very limited effect on the stability field. Retrograde reaction seems to be responsible for andalusite formation. Textural analyses show that the kyanite and andalusite relation is most likely a volume-for-volume replacement reaction (Kerrick, 1988). Andalusite may thus have inherited the isotopic composition of kyanite during retrogression. Retrograde reaction might have occurred more easily in the vein than in the host rock, due to preferential circulation of fluids within the discontinuity of the veins, as documented by the frequent retrogression of biotite into chlorite in the rim of the veins.

Acknowledgements

This work is part of a M.Sc. thesis by J.A. and X.M at the University of Lausanne (Institute of Mineralogy and Geochemistry, March 2003). We are grateful to Dr. C. de Capitani and Dr. B. Cesare for their helpful and constructive reviews. This paper benefited greatly from numerous discussions with, and corrections by Dr. Fraukje M. Brouwer, Dr. Alfons Berger and Dr. Edwin Gnos. We acknowledge assistance on the microprobes at the Institute of Mineralogy and Geochemistry at University of Lausanne and at the Institute of Geological Sciences at University of Berne, and during oxygen isotopes analysis at the Stable Isotope Laboratory at the University of Lausanne. We acknowledge the Swiss Nationalfonds (Grant 200021-103479/1) for financial support for the electron microprobe of Berne.

References

Abs-Wurmbach, I., Langer, K. and Schreyer, W. (1983): The influence of Mn^{3+} on the stability relations of the Al_2SiO_5 polymorphs with special emphasis on manganian andalusites (viridines), $(Al_{1-x}Mn_x^{3+})_2(O/SiO_4)$: an experimental investigation. *J. Petrol.* **24**, 48–75.

Berman, R. (1988): Internally-consistent thermodynamic data for minerals in the system Na_2O-K_2O-CaO-MgO-FeO-Fe_2O_3-Al_2O_3-SiO_2-TiO_2-H_2O-CO_2. *J. Petrol.* **29**, 445–522.

Berman, R. (1991): Thermobarometry using multi-equilibrium calculations: a new technique, with petrological applications. *Can. Mineral.* **29**, 833–855.

Berman, R. and Aranovich, L.Y. (1996): Optimized standard state and mixing properties of minerals: I. Model calibration for olivine, orthopyroxene, cordierite, garnet and ilmenite in the system FeO-MgO-CaO- Al_2O_3-SiO_2-TiO_2. *Contrib. Mineral. Petrol.* **126**, 1–24.

Cavosie, A.J., Sharp, Z.D. and Selverstone, J. (2002): Coexisting aluminium silicates in quartz veins: A quantitative approach for determining andalusite-sillimanite equilibrium in natural samples using oxygen isotopes. *Am. Mineral.* **87**, 417–423.

Cesare, B. (1994): Synmetamorphic veining: origin of andalusite-bearing veins in the Vedretto di Ries contact aureole. Eastern Alps, Italy. *J. metam. Geol.* **12**, 643–653.

Chamberlain, C.P. and Conrad, M.E. (1991): Oxygen isotope zoning in garnet. *Science* **254**, 403–418.

Chatterjee, N.D. and Froese, E. (1975): A thermodynamic study of the pseudobinary joint muscovite-paragonite in the system $KAlSi_3O_8$-$NaAlSi_3O_8$-Al_2O_3-SiO_2-H_2O. *Am. Mineral.* **60**, 985–993.

Chollet, N. (2000): Geologische Untersuchungen im Gebiet Sponda-Cognora (Simano-Decke, Ticino). Unpublished M. Sc. Thesis, University of Berne, Switzerland, 113 pp.

Codoni, A. (1981): Geologia e petrografia della regione del Pizzo di Claro. Ph. D. Thesis, Univeristy of Zürich, Switzerland, 179 pp.

Connolly, J.A.D. (1997): Devolatilization-generated fluid-pressure and deformation-propagated fluid flow during prograde regional metamorphism. *J. Geoph. Res.* **102**, 18149–18173.

Délèze, J.-Y. (1999): Géologie et minéralogie de la région du Cristallina (Pennique inférieur, NW du Tessin). Unpublished M. Sc. thesis, University of Lausanne, Switzerland, 288 pp.

Dyar, M.D., Lowe, E.W., Guidotti, C.V. and Delaney, J.S. (2002): Fe^{3+} and Fe^{2+} partitioning among silicates in metapelites: A synchrotron micro-XANES study. *Am. Mineral.* **87**, 514–522.

Dymek, R.F. (1983): Titanium, aluminium and interlayer cation substitutions in biotite from high-grade gneisses, West Greenland. *Am. Mineral.* **68**, 880–899.

Eiler, J.M., Valley, J.W. and Baumgartner, L.P. (1993): A new look at stable isotope thermometry. *Geochim. Cosmochim. Acta* **57**, 2571–2583.

Engi, M., Todd, C.S. and Schmatz, D.R. (1995): Tertiary metamorphic conditions in the eastern Lepontine Alps. *Schweiz. Mineral. Petrogr. Mitt.* **75**, 347–369.

Escher, A., Masson, H. and Steck, A. (1993): Nappe geometry in the Western Swiss Alps. *J. Struct. Geol.* **15**, 501–509.

Etheridge, M.A., Wall, V.J. and Cox, S.F. (1984): High fluid pressures during regional metamorphism and deformation: implications for mass transport and deformation mechanisms. *J. Geoph. Res.* **89**, 4344–4358.

Frey, M. and Ferreiro-Mählmann, R. (1999): Alpine metamorphism of the Central Alps. *Schweiz. Mineral. Petrogr. Mitt.* **79**, 135–154.

Fuhrman, M.L. and Lindsley, D.H. (1988): Ternary feldspar modeling and thermometry. *Am. Mineral.* **73**, 201–215.

Giletti, B.J. (1986): Diffusion effects on oxygen isotope temperatures of slowly cooled igneous and metamorphic rocks. *Earth Planet. Sci. Lett.* **77**, 218–228.

Grambling, J.A. and Williams, M.L. (1985): The effects of Fe^{3+} and Mn^{3+} on aluminium silicate phase relations in North-Central New Mexico, U.S.A. *J. Petrol.* **26**, 324–354.

Grujic, D. and Mancktelow, N.S. (1996): Structure of the northern Maggia and Lebendun Nappes, Central Alps, Switzerland. *Eclogae geol. Helv.* **89**, 461–504.

Guidotti, C.V. (1984): Micas in metamorphic rocks, *Rev. Mineral.* **13**, 357–455.

Guidotti, C.V. and Dyar, M.D. (1991): Ferric iron in metamorphic biotite and its petrologic and crystallochemical implications. *Am. Mineral.* **76**, 161–175.

Haar, C., Gallagher, J.S. and Kell, G.S. (1984): NBS/NRC Steam Tables. Thermodynamic and transport properties and computer programs for vapor and liquid states of water in SI units. Hemisphere Publishing Co., Washington, 271–276.

Henry, D.J. and Guidotti, C.V. (2002): Titanium in biotite from metapelitic rocks: Temperature effects, crystal-chemical controls, and petrologic applications. *Am. Mineral.* **87**, 375–382.

Hoernes, S. and Friedrichsen, H. (1980): Oxygen and hydrogen isotopic composition of alpine and prealpine minerals of the Swiss Central Alps. *Contrib. Mineral. Petrol.* **72**, 19–32.

Holland, T.J.B. and Powell, R. (1985): An internally consistent thermodynamic dataset with uncertainties and correlations: 2. Data and results. *J. metam. Geol.* **3**, 343–370.

Holland, T.J.B. and Powell R. (1998): An internally consistent thermodynamic data set for phases of petrological interest. *J. metam. Geol.* **16**, 309–343.

Huber, M., Ramsay, J. and Simpson, C. (1980): Deformation in the Maggia and Antigorio nappes – Lepontine Alps. *Eclogae geol. Helv.* **73**, 593–606.

Keller, F. (1968): Mineralparagenesen und Geologie der Campo Tencia—Pizzo Forno-Gebirgsgruppe. *Beitr. Geol. Karte Schweiz, Neue Folge* **135**, 72 pp.

Keller, F., Wenk, E., Bianconi, F. and Hasler, P. (1980): Pizzo Campo Tencia. Geol. Atlas Schweiz, 1:25000, Atlasblatt **73**, Kümmerley & Frey, Bern.

Kerrick, D.M. (1988): Al_2SiO_5-bearing segregations in Lepontine Alps, Switzerland: Aluminium mobility in metapelites. *Geology* **16**, 636–640.

Kerrick, D.M. (1990): Al_2SiO_5-bearing veins and segregations formed by crystallization within fractures and cavities. In: Kerrick, D.M., (Ed.). The Al_2SiO_5 polymorphs. *Rev. Mineral.* **22**, 325–345.

Kerrick, D.M. and Jacobs, G.K. (1981): A modified Redlich-Kwong equation for H_2O, CO_2 and H_2O-CO_2 mixtures at elevated pressures and temperatures. *Am. J. Sci.* **281**, 735–767.

Klein, H.-H. (1976): Aluminosilikatführende Knauern im Lepontin. *Schweiz. Mineral. Petrogr. Mitt.* **56**, 435–456.

Köppel, V., Günthert, A. and Grünenfelder, M. (1980): Patterns of U–Pb zircon and monazite in polymetamorphic units of the Swiss Central Alps. *Schweiz. Mineral. Petrogr. Mitt.* **61**, 97–119.

Kretz, R. (1983): Symbols for rock-forming minerals. *Am. Mineral.* **68**, 277–279.

Lacassin, R. (1988): Large-scale foliation boudinage in gneisses. *J. Struct. Geol.* **10**, 643–647.

Maeder, U.K. and Berman, R.G. (1991): A high pressure equation of state for carbon dioxide consistent with phase equilibrium and P-V-T data. *Am. Mineral.* **76**, 1547–1559.

Maxelon, M. (2004): Developing a three-dimensional structural model of the Lower Lepontine Nappes – Central Alps, Switzerland and Northern Italy. Ph. D. Thesis n° 15598, ETH Zürich, Switzerland, 209 pp.

Merle, O. and Le Gal, P. (1988): Post-amphibolitic westward thrusting and fold vergence in the Ticino domain. *Eclogae geol. Helv.* **81**, 215–226.

Moecher, D.P. and Sharp, Z.D. (1999): Comparison of conventional and garnet-aluminosilicate-quartz O isotope thermometry; insights for mineral equilibration in metamorphic rocks. *Am. Mineral.* **84**, 1287–1303.

Nabholz, W.K. and Voll, G. (1963): Bau und Bewegung im gotthardmassivischen Mesosoikum bei Ilanz (Graubünden). *Eclogae geol. Helv.* **56**, 756–808.

Passchier, C.W. (2001): Flanking structures. *J. Struct. Geol.* **23**, 951–962.

Platt, J.P. and Vissers, R.L.M., (1980): Extensional structures in anisotropic rocks. *J. Struct. Geol.* **2**, 397–410.

Powell, R. and Holland, T.J.B. (1985): An internally consistent thermodynamic dataset with uncertainties and correlations: 1. Method and a worked example, *J. metam. Geol.* **3**, 327–342.

Preiswerk, H. (1918): Geologische Bechreibung der Lepontinischen Alpen – zweiter Teil: Oberes Tessin und Maggiagebiet. *Beitr. Geol. Karte Schweiz* **26**, 80 p.

Putlitz, B., Valley, J.W., Matthews, A. and Katzir, Y. (2002): Oxygen isotope thermometry of quartz–Al_2SiO_5 veins in high-grade metamorphic rocks on Naxos island (Greece). *Contrib. Mineral. Petrol.* **143**, 350–359.

Ramsay, J.G. (1967): Folding and fracturing in rocks. McGraw-Hill, New-York, 568 pp.

Sauniac, S. and Touret, J. (1983): Petrology and fluid inclusions of a quartz-kyanite segregation in the main thrust zone of the Himalayas. *Lithos* **16**, 35–45.

Sepahi, A.A., Whitney, D.L. and Baharifar, A.A. (2004): Petrogenesis of andalusite-kyanite-sillimanite veins and host rocks, Sanandaj-Sirijan metamorphic belt, Hamadan, Iran, *J. metam. Geol.* **22**, 119–134.

Sharp, Z.D. (1992): In situ laser microprobe techniques for stable isotope analysis. *Chem. Geol.* **101**, 3–19.

Sharp, Z.D. (1995): Oxygen isotope geochemistry of the Al_2SiO_5 polymorphs. *Am. J. Sci.* **295**, 1058–1076.

Simpson, C. (1982): The structure of the northern lobe of the Maggia Nappe, Ticino, Switzerland. *Eclogae geol. Helv.* **75**, 495–516.

Spicher, A. (1972): Tektonische Karte der Schweiz, 1: 500000. Schweizerische Geologische Kommission, Basel.

Steck, A. (1984): Structures de deformations tertiaires dans les Alpes centrales (transversal Aar-Simplon-Ossola). *Eclogae geol. Helv.* **77**, 55–100.

Steck, A. (1998): The Maggia cross-fold: An enigmatic structure of the Lower Penninic nappes of the Lepontine Alps. *Eclogae geol. Helv.* **91**, 333–343.

Steck, A., Epard, J.-L., Escher, A., Gouffon, Y. and Masson, H. (2001): Carte tectonique des Alpes de Suisse occidentale et des régions avoisinantes 1:100000, Carte géologique spéciale n° 123, notice explicative - Office féd. Eaux Geologie (Berne), 73 pp.

Thompson, P.H. (1976): Isograd patterns and pressure-temperature distributions during regional metamorphism. *Contrib. Mineral. Petrol.* **57**, 277–295.

Todd, C.S. and Engi, M. (1997): Metamorphic field gradients in the Central Alps. *J. metam. Geol.* **15**, 513–530.

Trümpy, R. (1980): Pennic and lower nappes of Ticino (Lepontine Alps) In: Trümpy, R. (Ed.): Geology of Switzerland - a guide book. Part A: An outline of the geology of Switzerland. Wepf. and Co., Basel, 65–67.

Vannay, J-C., Sharp, Z.D. and Grasemann B. (1999): Himalayan inverted metamorphism constrained by oxygen isotope thermometry. *Contrib. Mineral. Petrol.* **137**, 90–101.

Walther, J.V. and Woodland, A.B. (1993): Experimental determination and interpretation of the solubility of the assemblage microcline, muscovite, and quartz in supercritical H_2O. *Geochim. Cosmochim. Acta* **57**, 2431–2437.

Wenk, E. (1970): Zur Regionalmetamorphose und Ultrametamorphose im Lepontin. *Fortschr. Mineral.* **47**, 34–51.

Wenk, E. and Keller, F. (1969): Isograde in Amphibolitserien der Zentralalpen. *Schweiz. Mineral. Petrogr. Mitt.* **49**, 157–198.

Woodland, A.B. and Walther, J.V. (1987): Experimental determination of the solubility of the assemblage paragonite, albite and quartz in supercritical H_2O. *Geochim. Cosmochim. Acta* **51**, 365–372.

Widmer, T. and Thompson, A.B. (2001): Local origin of high pressure vein material in eclogite facies rocks of the Zermatt-Saas zone, Switzerland. *Am. J. Sci.* **301**, 627–656.

Received 27 April 2005
Accepted in revised form 23 December 2005
Editorial handling: Reto Gieré